Anisotropy of Segregation at Grain Boundaries and Surfaces

PAUL WYNBLATT and DOMINIQUE CHATAIN

The purpose of this article is to review analytical models of the anisotropy of segregation to grain boundaries (GBs) and surfaces, and to evaluate their predictions. A summary of Gibbsian interfacial thermodynamics is provided as an introduction to the topic. This is followed by a historical overview of previous analytical models. A recently developed model of the dependence of GB segregation on the five macroscopic parameters of GB orientation is outlined, and illustration of how this formulation reduces to the particular cases of segregation to simpler types of interfaces is provided. In addition, some specific aspects of interfacial segregation, which have either been problematic or have lacked satisfactory explanation, are addressed. These include (a) the relationship between the compositions on the two sides of a given GB; (b) the difficulty of meaningful definitions of segregation-free energy (and related thermodynamic quantities such as enthalpy and entropy); (c) the so-called compensation temperature, at which the anisotropy of interfacial segregation seems to vanish; (d) the relationship between surface and GB segregation; and finally (e) an attempt to determine whether segregation increases or decreases interfacial energy anisotropy, and the consequences thereof on the equilibrium crystal shape of alloys. Where possible, comparisons are made with the results of experiments or computer simulations.

I. INTRODUCTION

THERE has been continuing interest in various phenomena associated with interfacial segregation, since the thermodynamic description of adsorption phenomena by Gibbs[1] over a century ago. From a materials perspective, interest has been driven by the impact of interfacial segregation on many important materials properties. For example, in the context of polycrystalline materials, grain boundary (GB) segregation can play a role in controlling such characteristics as crystallographic texture, the GB energy distribution, GB mobility, GB embrittlement, and electromigration processes. Segregation at materials surfaces can modify catalytic properties, influence equilibrium crystal shape, affect the work function, accelerate the rate of surface diffusion, and control sintering rates as well as other kinetic phenomena.

However, certain shortcomings of the Gibbsian thermodynamics of adsorption (described in more detail subsequently) prompted the later development of complementary analytical models of interfacial segregation, based on the concepts of statistical mechanics.[2–5] In the context of materials behavior, McLean[4] was the first to develop a model of that type, to deal explicitly with the phenomenon of GB segregation. Since that time, there has been a steady effort to develop improved analytical models for the prediction and interpretation of phenomena related to interfacial segregation in materials. Following the approach of McLean, the majority of these efforts have made use of the regular solution approximation, because of the simplicity it provides in the definition of the relevant model parameters, although other more sophisticated models have also been used from time to time.

PAUL WYNBLATT, Professor Emeritus, is with the Department of Materials Science and Engineering, Carnegie Mellon University, Pittsburgh, PA 15213. Contact e-mail: pw01@andrew.cmu.edu DOMINIQUE CHATAIN, Directeur de Recherches, is with CRMCN-CNRS, Campus de Luminy, 13288 Marseille, Cedex 9, France.

Manuscript submitted March 27, 2006.

One factor that has played a significant role in prompting the formulation of new analytical models of GB segregation has been the development of orientation imaging microscopy (OIM).[6] This technique has made it possible to characterize vast sets of grain boundaries (GBs) with respect to the five macroscopic degrees of freedom (DoFs) of GB orientation, sometimes referred to as the GB character. Whereas computer simulation remains an important approach for predicting GB properties,[7] it cannot currently be used to predict the behavior of GBs over the vast five-dimensional space represented by the five DoFs, hence, the need for analytic techniques with the capability of calculating GB properties.

Although OIM studies cannot directly reveal the presence or absence of segregation at GBs, they do provide indirect information in the form of GB orientation frequency distributions.[8,9] Furthermore, it is now well established that the GB frequency distribution in a material is inversely related to the prevailing GB energy anisotropy,[6,10,11] which depends in turn on the anisotropy of segregation through the Gibbs adsorption isotherm. Thus, the recent development of analytical models that are capable of evaluating both GB energy and GB composition, as a function of the macroscopic orientation parameters,[12,13] has yielded new tools for interpreting the connection between OIM data and GB segregation.[9] Whereas these models are somewhat simplistic, in that they rely on nearest-neighbor bond concepts, they have been shown to predict GB segregation behavior that agrees surprisingly well with more sophisticated Monte-Carlo–based computer simulations.[13]

The purpose of this article is to review analytical models of interfacial segregation and to illustrate their value by comparing the predictions to results obtained by either experimental or computer simulation techniques.

The topic will be introduced by providing a summary of Gibbsian interfacial thermodynamics, as well as a historical overview of analytical models. The most recent analytical model for GBs will be outlined, and it will be shown that this formulation reduces to the particular cases of

segregation to simpler types of interfaces (such as liquid-vapor interfaces and solid-vapor interfaces with anisotropy). In addition, some specific aspects of interfacial segregation, which have either been problematic or have lacked satisfactory explanation, will be addressed. These include the following:

the relationship between the compositions on the two sides of a given GB;
the difficulty of meaningful definitions of segregation free energy (and related thermodynamic quantities such as enthalpy and entropy);
the so-called compensation temperature, at which the anisotropy of interfacial segregation seems to vanish;
the relationship between surface and GB segregation; and, finally,
an attempt to determine whether segregation increases or decreases interfacial energy anisotropy, and the consequences thereof on the equilibrium crystal shape of alloys.

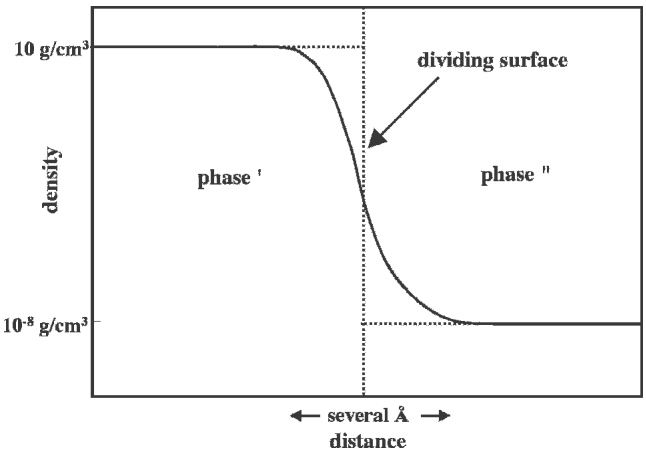

Fig. 1—Schematic of density variation across a solid-vapor interface.

II. INTERFACE THERMODYNAMICS

A. *Interfacial Excess Properties*

The interfacial energy is denoted by γ and is defined as the reversible work needed to create unit area of surface, at constant temperature, volume (or pressure), and chemical potentials. We begin by reviewing the thermodynamics of interfaces, using the liquid-vapor surface as an example, and ignoring effects of surface curvature. Thus, this treatment applies strictly only to planar fluid surfaces.

Following Gibbs,[1,14,15] we consider a system composed of a liquid and a vapor phase at equilibrium, separated by an interface. Physical interfaces are generally not perfectly sharp on an atomic scale. Thus, any property we measure in the two phases and across the interface will show some transition region, *e.g.*, in a plot of density across the interface, as shown in Figure 1.

We define a *hypothetical system*, which consists of two phases that are uniform in properties up to a plane called the *dividing surface*. The properties of the real system follow the solid lines and the hypothetical system properties follow the dashed lines. Thus, the properties of each phase in the hypothetical system take on values corresponding to the bulk values, far from the interface, and each phase is assumed to be homogeneous up to the dividing surface. The thermodynamic properties of the *real system* over and above those of the hypothetical system are termed *surface* or *interfacial excess properties*, *i.e.*, we assign to the interface any excess of the thermodynamic properties of the real system over those of the hypothetical system.

As an example, we write the interfacial excess internal energy of the system, E^s, as

$$E^s = E - E' - E'' \qquad [1]$$

where E is the real system internal energy, E' is the internal energy of phase $'$, and E'' is the internal energy of phase $''$. This shows how the excess property is just the property of the real system, less the properties of the bulk phases (hypothetically extended to the dividing surface). It is important to note that the position of the dividing surface is arbitrary. It can be placed at any convenient location within the bounds of the physically diffuse region. Some consequences of this arbitrariness are addressed subsequently.

Every thermodynamic property of the system can be written in the same way as in Eq. [1], *e.g.*, the number of moles of component i in the real system is expressed as: $n_i = n_i' + n_i'' + n_i^s$. The only exception is that the volume of the system is written $V = V' + V''$; *i.e.,* there is no volume associated with the surface.*

*The Gibbsian approach, which deliberately ignores interfacial excess volume, may seem to pose a problem in the case of GBs where free volume is often considered to be an important property. This apparent problem can be circumvented by considering that the interface contains an excess of vacancies, with vacancies treated explicitly as a component of the system.[10]

The internal energy of any phase (say, phase $'$) is conveniently considered to be a function of the extensive variables entropy, S', volume, V', and number of moles, n'_i. Then,

$$dE' = \left(\frac{\partial E'}{\partial S'}\right)_{V',n'_i} dS' + \left(\frac{\partial E'}{\partial V'}\right)_{S',n'_i} dV' + \sum_i \left(\frac{\partial E'}{\partial n'_i}\right)_{S',V',n'_{i\neq i}} dn'_i$$

or

$$dE' = TdS' - PdV' + \sum_i \mu_i' dn'_i \qquad [2]$$

where T is the temperature, P is the pressure, and μ_i' is the chemical potential of component i in the $'$ phase. This is the standard expression for the internal energy of a single uniform phase containing more than one component. Similarly, the energy of phase $''$ is

$$dE'' = TdS'' - PdV'' + \sum_i \mu_i'' dn''_i \qquad [3]$$

For the surface, which does not have any volume, the excess internal energy is written as

$$dE^s = TdS^s + \gamma dA + \sum_i \mu_i^s dn_i^s \quad [4]$$

This shows that in the expression for the surface excess internal energy, the *PdV* term is replaced by a term consisting of the surface energy multiplied by a change in area. Since, for a system in equilibrium, the chemical potential must be equal everywhere, we impose the condition $\mu_i' = \mu_i'' = \mu_i^s$. Substituting for dE', dE'', and dE^s into Eq. [1], we obtain

$$dE = T(dS' + dS'' + dS^s) - P(dV' + dV'') + \gamma dA + \sum_i \mu_i \left(dn'_i + dn''_i + dn_i^s\right)$$

or

$$dE = TdS - PdV + \gamma dA + \sum_i \mu_i dn_i \quad [5]$$

This is an important result. It shows that in the limit of a system where the contribution of the surface energy is small with respect to the bulk energy, the γdA term becomes negligible and Eq. [5] reduces to the standard thermodynamic expression for the internal energy. All other thermodynamic properties of a system with a surface can be derived from this expression.

The Helmholtz free energy is given by $F = E - TS$, and its derivative may be written as

$$dF = dE - TdS - SdT = -SdT + PdV + \gamma dA + \sum_i \mu_i dn_i \quad [6]$$

The corresponding interfacial excess quantity is then

$$dF^s = -S^s dT + \gamma dA + \sum_i \mu_i dn_i^s \quad [7]$$

Similarly, the Gibbs free energy, which is written $G = E + PV - TS$, yields

$$dG = dE + PdV + VdP - TdS - SdT = -SdT + VdP + \gamma dA + \sum_i \mu_i dn_i \quad [8]$$

and

$$dG^S = -S^S dT + \gamma dA + \sum_i \mu_i dn_i^s \quad [9]$$

B. *Gibbs Adsorption Equation*

We now go back to Eq. [4], in which dE^s is expressed in terms of extensive-independent variables only (dS^s, dA, dn_i^s) while the intensive variables (T, γ, μ_i) are constant in the equilibrated system. Thus, we can integrate Eq. [4] to obtain

$$E^s = TS^S + \gamma A + \sum_i \mu_i n_i^s \quad [10]$$

Redifferentiating this result yields

$$dE^S = TdS^S + S^S dT + \gamma dA + Ad\gamma + \sum_i \mu_i dn_i^s + n_i^s d\mu_i$$

However, by Eq. [4],

$$dE^S = TdS^S + \gamma dA + \sum_i \mu_i dn_i^s$$
$$\therefore S^S dT + Ad\gamma + \sum_i n_i^s d\mu_i = 0 \quad [11]$$

(This procedure for obtaining Eq. [11] is analogous to that used in the derivation of the Gibbs–Duhem equation). We now define the following new quantities:

$$s^s \equiv S^s/A, \text{ and } \Gamma_i \equiv n_i^s/A$$

Quantities expressed per unit area are known as *specific surface excess quantities*, *e.g.*, s^s is known as the specific surface excess entropy, and Γ_i is the specific surface excess number of moles of component *i*. However, to avoid this cumbersome nomenclature, Γ_i is generally referred to simply as the *adsorption*. With these definitions, we can rewrite Eq. [11] as

$$d\gamma = -s^s dT - \sum_i \Gamma_i d\mu_i \quad [12]$$

This is the well-known *Gibbs adsorption equation*. It gives the variation of γ with changes in T and μ_i, which can easily be related to the composition of the bulk phases.

Now that adsorption has been defined, it is useful to digress briefly on the relationship between interfacial adsorption and segregation. This issue has been discussed previously, for example, by Hondros and Seah.[16] The phenomenon of adsorption from a gas phase onto the surface of a solid was well known long before any knowledge about phenomena such as surface or GB segregation was available. To illustrate the connection between adsorption and segregation, consider the following two thought experiments. In the adsorption thought experiment, a solid is placed in contact with a gas whose atoms or molecules have a tendency to stick to the solid surface. Under these conditions, an excess of those molecules will build up at the surface. Depending on the temperature at which this adsorption process is observed, the gas species may or may not be able to equilibrate with the solid, *i.e.*, to diffuse into the solid until the solid is saturated with the vapor species at the pressure of the experiment. The Gibbsian formalism described previously applies strictly only to systems in equilibrium, *i.e.*, ones where the chemical potential of the gas (or adsorbing) species is uniform throughout the gas, the interface region, and the solid (refer to the discussion on equality of chemical potentials preceding Eq. [5]).

Under those circumstances, Eq. [12] will be valid, and the surface excess of the adsorbed species, Γ, will be well defined.

Segregation is generally studied in cases where the segregating species is present in the solid. In the segregation thought experiment, a piece of solid containing the dissolved gas species is placed in an evacuated closed container and is allowed to equilibrate. The dissolved species will then redistribute between the gas phase, the interface, and the solid. If by appropriate selection of the solute concentration, the volume of the container, *etc.*, the final pressure in the container is the same as in the adsorption experiment, the excess of the gas species at the surface will, of course, also be the same. From the standpoint of the interface, it does not matter whether the adsorbed species originated from the gas phase or from the solid. In this sense, the terms segregation and adsorption mean exactly the same thing. However, the energy changes associated with the two processes will be different because they are not defined in the same manner. The adsorption energy is generally defined in terms of changes resulting from the transfer of a gas atom or molecule to the interface, whereas the segregation energy is defined in terms of changes associated with transfer from the bulk of the condensed phase to the interface.

We now return to Eq. [12]. At constant temperature, this equation simplifies to the Gibbs adsorption isotherm. In the case of a two-component system, we can write

$$d\gamma = -\Gamma_1 d\mu_1 - \Gamma_2 d\mu_2 \qquad [13]$$

Now, the Gibbs—Duhem equation for one of the two bulk phases, say, phase $'$, can be expressed as

$$n'_1 d\mu_1 + n'_2 d\mu_2 = 0 \qquad [14]$$

which is valid either at constant T and P or at constant T and V. Equation [14] can be used to eliminate one of the chemical potentials in Eq. [13]. By convention, the chemical potential of the solvent (majority component, labeled 1) is eliminated, and the Gibbs isotherm is rewritten in terms of the solute (minority component, labeled 2):

Thus,

$$\frac{d\gamma}{d\mu_2} = \left(\Gamma_1 \frac{n'_2}{n'_1} - \Gamma_2\right) \qquad [15]$$

Here, $d\gamma/d\mu_2$ is a measurable quantity, and therefore *cannot* depend on an arbitrary choice of the dividing surface. On the other hand, Γ_1 and Γ_2 do depend on the position of the dividing surface. Thus, the right-hand side (rhs) of Eq. [15], $(\Gamma_1 n'_2/n'_1 - \Gamma_2)$, *i.e.*, this particular combination of adsorption variables, must also be independent of the position of the dividing surface.

In the case of interfaces between a condensed phase and a vapor phase (*e.g.*, liquid-vapor or solid-vapor interfaces), the difference in density across the interface makes it possible to select the position of the Gibbs dividing surface so as to make one of the adsorption terms vanish. In those cases, Eq. [15] can be simplified, for example, by choosing the position of the dividing surface so as to make $\Gamma_1 = 0$. Under these conditions, Γ_2 is no longer arbitrary (since we have now made a specific choice for the position of the dividing surface) and is written $\Gamma_{2,1}$ to indicate that the choice $\Gamma_1 = 0$ has been made:

$$d\gamma/d\mu_2 = -\Gamma_{2,1} \qquad [16]$$

where $\Gamma_{2,1}$ is sometimes referred to as the *relative adsorption*.[5] The value of $\Gamma_{2,1}$ (or of any adsorption term) can be either positive or negative. From Eq. [16], it can be seen that if the adsorption of component 2 is positive (*i.e.,* there is a positive excess of component 2 at the surface of the condensed phase), then $d\gamma/d\mu_2$ will be negative, and the surface energy of the solid will decrease as the chemical potential, and hence the bulk concentration of component 2, increases. However, the simplification shown here for the case of interfaces between a condensed phase and a vapor cannot be applied to grain boundaries or other interfaces between two condensed phases. Thus, in those cases, more complete versions of the Gibbs adsorption isotherm, such as Eqs. [13] or [15], must be used.

The term $d\mu_2$ in Eq. [15] or [16] can be transformed using the definition of chemical potential in terms of activity, a: $\mu_2 = \mu_2^\circ + \mathrm{k}T \ln a_2$, where μ_2° is the chemical potential in the standard state. In the case of ideal solutions, Raoult's law can be applied: $a_2 = X_2$, where X_2 is the atom fraction (or mole fraction) of the solute; and in dilute solutions, Henry's law, $a_2 = \mathrm{k_o} X_2$, where $\mathrm{k_o}$ is a constant, can be applied. In either case, $d\mu_2 = \mathrm{R}T\, d(\ln X_2)$. Therefore, in these particular limits, the preceding relationships may be simplified as

$$\frac{1}{RT}\frac{d\gamma}{d\ln X_2} = \left(\Gamma_1 \frac{n'_2}{n'_1} - \Gamma_2\right) \qquad [17]$$

or

$$\frac{1}{RT}\frac{d\gamma}{d\ln X_2} = -\Gamma_{2,1} \qquad [18]$$

Thus, we can obtain the adsorption $\Gamma_{2,1}$ (which is related to the interfacial composition) from the dependence of the surface energy on bulk composition. In principle, we can also obtain the change in surface energy that results from the adsorption of solute. To do this, it is necessary to integrate the Gibbs isotherm, which requires some knowledge of the dependence of $\Gamma_{2,1}$ on X_2. Unfortunately, Gibbsian thermodynamics do not provide a suitable functional form for $\Gamma_{2,1}(X_2)$. In later sections, we will develop models that provide this needed functional relationship.

C. *Relation between* γ *and Surface Free Energy*

Integrating Eq. [7], and dividing by the area of the surface, A, it is possible to write

$$f^s = F^s/A = \gamma + \sum_i \mu_i \Gamma_i \qquad [19]$$

where f^s is the specific surface excess Helmholtz free energy. Similarly, from Eq. [9],

$$g^s = G^s/A = \gamma + \sum_i \mu_i \Gamma_i \quad [20]$$

We see from these relations that, strictly speaking, the surface energy *of a multicomponent solution* is equal to neither the specific surface excess Gibbs nor the Helmholtz free energies. However, for the *surface energy of a liquid or solid in a single component system* (*i.e.*, a pure substance), it is possible to select the dividing surface such that $\Gamma_1 = 0$. For these cases only, $\gamma = f^s = g^s$. Thus, in multicomponent systems, it is best to avoid the terminology of *interfacial free energy*. From the preceding expressions, it is possible to write the surface energy of a multicomponent system in terms of the free energies, as follows:

$$\gamma = f^s - \sum_i \mu_i \Gamma_i \quad [21]$$

$$\gamma = g^s - \sum_i \mu_i \Gamma_i \quad [22]$$

The thermodynamic potential ($F - \Sigma_i \mu_i n_i$) is known as the *grand potential* (it is also sometimes referred to as the *Kramer's potential*). Thus, we see from Eq. [21] that the surface energy is equal to the surface excess grand potential per unit area. This will prove to be a very useful definition in subsequent sections.

III. BRIEF HISTORICAL OVERVIEW OF ANALYTICAL MODELS

A. *Background*

We have seen that the Gibbs adsorption isotherm relates the adsorption to the variation of interfacial energy with bulk composition [$\Gamma_{2,1} = -d\gamma/d\mu_2$]. However, there are several features that detract from the usefulness of this relation.

- Neither γ nor its variation with composition is easy to measure in solids.
- $\Gamma_{2,1}$ is difficult to measure directly, because interfacial composition profiles can extend some distance from the interface, and one must determine the composition profiles of both components in the most general case.
- Unless the relationship between $\Gamma_{2,1}$ and μ_2 is known, the Gibbs adsorption isotherm cannot be integrated.

For these reasons, alternative approaches have been sought to complement the Gibbsian formalism. These approaches have made use of the concepts of statistical thermodynamics and go back to the work of Langmuir,[17] Fowler and Guggenheim,[2] and Ono and Kondo.[3]

B. *The McLean Model*

In the materials literature, the first treatment of interfacial segregation was put forward by McLean for the case of GBs.[4] That formalism has also been used extensively to interpret surface segregation phenomena. Like most other treatments, McLean's model used a monolayer representation of the interface. As was later pointed out by Defay *et al.*,[5] models that employ a monolayer interface are not strictly consistent with Gibbsian adsorption, *i.e.*, interfaces must be represented by a multilayer formalism in order to be compatible with the Gibbs formalism. In his model, McLean also adopted a regular solution approximation, in which the free energy of the system (bulk plus interface) was assumed to consist of an entropy of mixing contribution, written in the ideal solution limit, and a nonzero enthalpy (or energy) of mixing contribution. In the regular solution approximation, the species in the interfacial and bulk regions are thus assumed to be randomly distributed, and the total entropy (in a binary system consisting of a solvent and one solute) is written as

$$\begin{aligned} S_{id} = &- R[n^s x^s \ln x^s + n^s(1-x^s)\ \ln(1-x^s) \\ &+ Nx \ln x + N(1-x)\ \ln(1-x)] \end{aligned} \quad [23a]$$

where x^s and x are the atom fractions,* and n^s and N are the numbers of atoms, of the segregating component in the interface and the bulk, respectively. Whenever this ideal solution entropy approximation is used, the resulting expression for the composition of the interface displays the following form:

$$\frac{x^s}{1-x^s} = \frac{x}{1-x} \exp\left\{-\frac{\Delta H_{\text{seg}}}{RT}\right\} \quad [23b]$$

where ΔH_{seg} is the enthalpy of segregation. For a substitutional solution, ΔH_{seg} represents the enthalpy change associated with the exchange of a segregant atom in the bulk with an atom of the other species located at the interface. It should be noted that x^s is not identical with the Gibbsian Γ. The relation between these quantities is

$$\Gamma = (x^s - x)/\sigma \quad [24]$$

where σ is the area per mole at the (monolayer) interface.

McLean assumed that the driving force for segregation was the complete elimination of the bulk elastic strain energy, ΔE_{el} (defined as a positive quantity), associated with a misfitting solute atom in the matrix of the solvent, when a solute atom in the bulk is exchanged with a solvent atom in the surface, *i.e.*,

$$\Delta H_{\text{seg}} = -\Delta E_{el} \quad [25]$$

Since only the solute can segregate to the interface in McLean's model, x^s necessarily represents the atom fraction of solute at the interface. However, the segregating species is not always the solute, as it is possible for the solvent to segregate (a case that is sometimes referred to as desegregation, and which is equivalent in the Gibbsian

*We shall use the symbol x^S to describe the atom fraction of segregant whenever the interfacial deviation in composition is assumed to be restricted to a single monolayer. When the variation is assumed to extend over several atomic layers, the symbol x^i will be used for the atom fraction of segregant in the ith atomic layer.

description to a negative value of Γ for that component). Expressions such as Eq. [23b], resulting from the McLean model, are formally similar to the Langmuir isotherm. As a result, the McLean model is often referred to as the Langmuir–McLean model.

C. *The Defay and Prigogine Model*

Defay *et al.*[5] applied a regular solution formalism to the computation of the equilibrium composition of a liquid surface. Their model employed a nearest neighbor bond description to calculate the enthalpy of the system (bulk plus interface) and assumed that the atoms of the liquid resided on the points of a lattice, *i.e.*, they chose a solidlike model of the liquid. In addition, they took the surface to consist of a single plane of atoms in equilibrium with a semi-infinite bulk. Their result may be expressed as

$$\Delta H_{\text{seg}} = (\gamma_{\text{B}} - \gamma_{\text{A}})\,\sigma + 2\omega\left[z^{\ell}(x - x^{s}) + z^{v}(x - \tfrac{1}{2})\right] \quad [26]$$

where γ_{A} and γ_{B} are the surface energies of the pure A and B components in the binary solution (component B taken to be the solute), and ω is the regular solution parameter for the AB solution. The term ω is defined as $\omega = \varepsilon_{\text{AB}} - (\varepsilon_{\text{AA}} + \varepsilon_{\text{BB}})/2$, where ε_{AB}, ε_{AA}, and ε_{BB} (taken to be negative quantities) are the energies of bonds connecting A-B, A-A, and B-B neighboring pairs of atoms, respectively. The terms z^{ℓ} and z^{v} are the numbers of in-plane bonds and half of the out-of-plane bonds of an atom in the surface plane, such that the total coordination number of an atom in the system is given by $z = z^{\ell} + 2z^{v}$. Finally, the atom fractions x and x^{S} are also taken to relate to the solute, component B. One important difference between Eqs. [25] and [26] should be noted. In Eq. [26], the enthalpy of adsorption depends on the fraction of segregated species at the interface, whereas in Eq. [25], it is a constant. The origin of expressions such as Eq. [26] will be discussed below in Section IV.

D. *The Wynblatt and Ku Model*

As was pointed out by Burton and Machlin,[18] neither the McLean nor the Defay *et al.* type models are able to provide even qualitatively correct predictions of the segregating component at binary solid alloy surfaces. The reason is that the model of Defay *et al.* considers only ''chemical'' contributions to the heat of segregation, whereas McLean ignores all but ''elastic'' contributions. While the neglect of elastic effects by Defay and Prigogine was appropriate in a model intended to represent the surface behavior of liquid solutions, its application to solid solutions requires modifications to include the elastic effects considered by McLean. These considerations were first recognized by Wynblatt and Ku.[19,20] As a result, they proposed a combined model in which the chemical and elastic contributions to the heat of segregation of Eqs. [25] and [26] were simply added, to yield

$$\Delta H_{\text{seg}} = (\gamma_{\text{B}} - \gamma_{\text{A}})\,\sigma + 2\omega\left[z^{\ell}(x - x^{s}) + z^{v}(x - \tfrac{1}{2})\right] - \Delta E_{el} \quad [27a]$$

in which the elastic strain energy was written according to a continuum linear elastic formalism due to Friedel:[21]

$$\Delta E_{el} = \frac{24\pi K_2 G_1 r_2 (r_1 - r_2)^2}{3Kr_2 + 4Gr_1} \quad [27b]$$

where K_2 is the bulk modulus of the solute, G_1 is the shear modulus of the solvent, and r_2 and r_1 are the atomic radii of the pure solute and solvent atoms, respectively. When this combined form of the heat of segregation was inserted into Eq. [23b], it produced predictions of the segregating component in binary solid solutions that were qualitatively correct over the data available at that time.[20]

The combined model showed that there are three principal contributions responsible for segregation to the surfaces of solid metallic alloys. The chemical driving force, illustrated in Eq. [26], really includes two distinct contributions, a term that depends on the difference between the surface energies of the pure components (*i.e.*, a surface energy driving force) and a term that depends on the regular solution constant (*i.e.*, an interatomic interaction driving force). The latter vanishes in the case of ideal solutions (for which $\omega = 0$). The third driving force is the one identified by McLean, namely, an elastic strain energy contribution associated with the degree of misfit of the solute in a solution. This term will also vanish in an ideal solution.

The extent of segregation depends not only on the magnitude of the three contributions mentioned previously, but also on their signs. Negative contributions to the heat of segregation increase the value of x^{s} in Eq. [23b], whereas positive ones decrease x^{s}. Since ΔE_{el} (Eq. [27b]) is always positive, the solute strain energy contribution to the heat of segregation will always favor solute segregation. In contrast, the two chemical terms can be either positive or negative for the solute. The surface energy of the pure solute can be either greater or smaller than that of the solvent, and a smaller surface energy for a given component will tend to promote segregation of that component. Similarly, a positive regular solution constant, ω, will add to the driving force for solute segregation. Thus, it is the sign of ΔH_{seg}, *i.e.*, of the sum of the three contributions, that will determine whether the solute or the solvent will tend to segregate to the interface. Furthermore, segregation will be strongest when the three contributions are all negative.

E. *The Lee and Aaronson Model*

Several refinements of these models were subsequently proposed. One important improvement was made by Lee and Aaronson,[22,23] who first addressed the effects of surface structural and energy anisotropy. Although the model of Defay *et al.* displays some features of anisotropy, through the coordination number terms, z^{ℓ} and z^{v}, which can change with surface orientation, their model is one in which the broken bonds (that account for the surface energy) are all associated with atoms in the first plane of surface atoms. For example, in the case of fcc crystals, this means that only (111) and (100) surfaces can be described by the Defay *et al.* model, as all other (*hkl*) surface orientations have atoms with broken bonds in deeper atom planes. Lee and Aaronson developed a multilayer

formalism, which accounts for all atoms with broken bonds at any surface orientation (*hkl*) in an fcc crystal. This allows the calculation of equilibrium near-surface composition over any number of atom planes, for any surface orientation. Among others, it also means that the maximum segregation is no longer restricted to one monolayer of segregant, as was the case in models such as McLean's.

F. *Entropy Considerations*

All of the regular solution-based models suffer from the deficiency that the entropy is written in a form that assumes ideal random mixing of the atoms (both in the bulk and in each atom plane of the near-surface region). In addition, the energy terms are also based on the assumption of a random distribution of the different species. In this regard, the regular solution approximation is similar to the Bragg–Williams (BW)[24] treatment of long-range order in solids, where the formulation of both energy and entropy assumes a random distribution of the atomic species on each sublattice; hence, the occasional reference to these models in the literature as being based on the BW approximation. Several attempts have been made at different times to introduce more realistic entropy descriptions. Wynblatt and Ku[20] proposed a method for calculating the excess entropy change upon segregation, $\Delta S_{\text{seg}}^{XS}$, so as to allow reformulation of Eq. [23b] into the form

$$\frac{x^s}{1-x^s} = \frac{x}{1-x}\exp\left\{\frac{\Delta S_{\text{seg}}^{XS}}{R}\right\}\exp\left\{-\frac{\Delta H_{\text{seg}}}{RT}\right\} = \frac{x}{1-x}\exp\left\{-\frac{\Delta F_{\text{seg}}^{XS}}{RT}\right\} \quad [28]$$

It should be emphasized that the excess entropy of segregation reflects all entropy changes above and beyond the ideal entropy of mixing, which is already included, and which leads to the exponential form of Eqs. [23b] and [28]. The excess entropy of segregation can be formulated by an approach analogous to that used to write ΔH_{seg} in Eq. [27a], if one recognizes that the regular solution constant may be expressed in terms of the enthalpy of mixing, ΔH_m, of the solution $\omega = \Delta H_m/[zx(1-x)]$; *i.e.*,

$$\Delta H_{\text{seg}} = (\gamma_{\text{B}} - \gamma_{\text{A}})\,\sigma + \frac{2\Delta H_m}{zx(1-x)}\left[z(x-x^s) + z^v\left(x-\tfrac{1}{2}\right)\right] - \Delta E_{el} \quad [29a]$$

Then, the excess entropy of segregation may be written as[19,20]

$$\Delta S_{\text{seg}}^{XS} = (S_{\text{B}} - S_{\text{A}})\,\sigma + \frac{2\Delta S_m^{XS}}{zx(1-x)}\left[z(x-x^s) + z^v\left(x-\tfrac{1}{2}\right)\right] - S_{el} \quad [29b]$$

where S_{A} and S_{B} are the temperature dependences of the interfacial energies of the pure components (B taken to be the solute), ΔS_m^{XS} is the excess entropy of mixing, and S_{el} is an elastic entropy that may be computed from the temperature dependence of the elastic constants of Eq. [27b]. Therefore, the excess entropy of segregation also has two chemical contributions and one elastic contribution, just as the corresponding enthalpy. These three terms can either all be of the same sign, and reinforce each other, or have different signs and partially cancel out. In general, the absolute value of the excess entropy of segregation will be large when the enthalpy of segregation has a large absolute value, and *vice versa*.

Efforts were also made to account for deviations from random mixing in segregated systems, for example, by Kumar *et al.*[25] and by Moran-Lopez and Falicov.[26,27] However, these formulations, as well as Eq. [29b], require knowledge of parameters that are difficult to evaluate, and have therefore not been used extensively. In this context, it is also worth mentioning the development of approaches using the cluster variation method.[28,29,30]

More recently, Polak and Rubinovich[31] have developed a surface segregation formalism, referred to as the *free energy expansion method*, in which they allow for deviations from the random distribution of species on a site by site basis in the near-surface region. This approach has turned out to be very useful for describing both long- and short-range order phenomena at segregated alloy surfaces.

G. *Related Models*

Several other models of interfacial segregation that have employed a similar formalism, but which lie outside the scope of this review, are worth mentioning for the sake of completeness. They include models of segregation to interfaces in ionic materials, to surfaces and GBs in ternary alloys, and to interphase boundaries in alloys.

Regular solution-type models have been used to treat interfacial segregation in ionic solids. In general, there is an electrostatic potential difference between an interface and the bulk of an ionic crystal, as well as a space charge in the near-interface region. As a result, it is necessary to include consideration of these electrostatic effects when computing the distribution of chemical species at and near an interface.[32,33] The interfacial segregation of impurity ions, especially those that differ in valence from the ions of the host solvent, will be subject to the driving forces similar to those mentioned previously for other materials (interfacial energy differences between the pure solute and solvent, interionic interactions, and solute misfit strain energy) plus additional electrostatic terms.[34,35]

Some significant effort has been devoted to applications of the regular solution approach to interfacial segregation in ternary solid solutions.[36–38] Work on three component systems was pioneered by Guttmann and co-workers[36,37] and was driven by interest in the possible interactions between segregating solute species (such as cosegregation and site competition effects) in the context of temper embrittlement phenomena at GBs in steels. In this article, we will focus on the segregation behavior of binary systems, and omit discussion of these multicomponent effects.

Finally, the regular solution formalism has been applied to segregation at interphase boundaries in alloys. Because of the phase diagram symmetry imposed on two-component systems by the regular solution approximation, no excess interfacial composition can be predicted by this

approach in binary systems. Nevertheless, it is possible to use this approach to produce useful predictions of interphase boundary composition in ternary alloys.[38–41]

IV. A MODEL OF INTERFACIAL SEGREGATION

A. *Introductory Comments*

We begin by describing a model of the equilibrium composition of a GB characterized by the five macroscopic orientation parameters. This model is based on two earlier pieces of work: (1) a multilayer *surface* segregation model[42] and (2) a semiempirical GB energy model in pure materials written in terms of the five macroscopic DoF's.[12] The latter has recently been used with some considerable success to rationalize the results of GB wetting experiments in polycrystalline alloys.[12] Both of these earlier models have relied on the prior work of Lee and Aaronson.[22,23] Once expressions for the equilibrium composition of a GB have been developed, the model can be particularized to several of the other cases that have been treated previously, such as segregation to crystalline surfaces of orientation (*hkl*), to segregation at liquid surfaces, *etc*.

Two general approaches can be used to calculate the composition of a near-interface region. In the first approach, an expression is written for the free energy of the entire system, consisting of bulk phases separated by an interface. This expression is then minimized with respect to the compositions of the bulk and interface regions. Since the free energy is the appropriate thermodynamic potential for a closed system, its minimization must be performed under the constraints of atomic species conservation, using variational calculus techniques such as Lagrangian multipliers, to account for the transfer of atoms between the bulk and the interface. Although minimization of the system free energy has been used widely, it has sometimes not properly accounted for mass conservation. As a result, it is probably preferable to perform calculations of the equilibrium composition of the interface using the second approach, which involves minimization of the interfacial excess grand potential, a quantity that was shown previously (Eq. [21]) to be identical with the interfacial energy. This thermodynamic potential is suitable for open systems. Conceptually then, the system is considered to be the interface. The interface is in contact with the bulk, which acts as an infinite reservoir of the components, at a properly specified chemical potential. We shall employ the latter approach in Section B.

B. *GB Segregation Model*

Two semi-infinite fcc crystals are considered. Each crystal consists of atoms located on the lattice points of planes of orientation (*hkl*) terminating at the GB. In general, the crystals on either side of the GB will be terminated by different (*hkl*) planes (referred to as $(hkl)_1$ and $(hkl)_2$), and will be rotated with respect to each other by a twist angle, ϕ, about an axis perpendicular to the GB plane. The five macroscopic orientation parameters of the GB are then taken to be the two variables required to define each of the two terminating (*hkl*) planes, and the twist angle, as shown schematically in Figure 2. This method of defining the DoF's has been referred to as the *interface plane scheme*.[43,44,45]

The indices of the terminating planes must be chosen such that $h \geq k \geq l$, and be reduced to the lowest integers. The (*hkl*) planes in each crystal are numbered by an index i, where $i = 1$ identifies the terminating plane at the GB. It is also necessary to define a second index, j, which counts the planes from any given plane i. The maximum value of j is denoted by J_{max}, and represents the farthest plane containing nearest neighbors of atoms in the ith plane. It is defined by $J_{max} = (h + k)/2$ when h, k, and l are all odd and $J_{max} = (h + k)$ for mixed h, k, and l. The indices i and j are illustrated in the schematic of Figure 3 and are also explained in greater detail in the article of Lee and Aaronson.[22,23]

We consider an fcc binary A-B substitutional solid solution in which the solute species is taken to be component B. The composition of the ith atom plane on one side of the GB will have the same form as that of Eq. [23b]:

$$\ln \frac{x^i}{1 - x^i} = \ln \frac{x}{1 - x} - \frac{\Delta H^i_{seg}}{RT} \qquad [30]$$

where x^i and x are the atomic fractions of the component B in the ith atomic plane and in the bulk, respectively, and

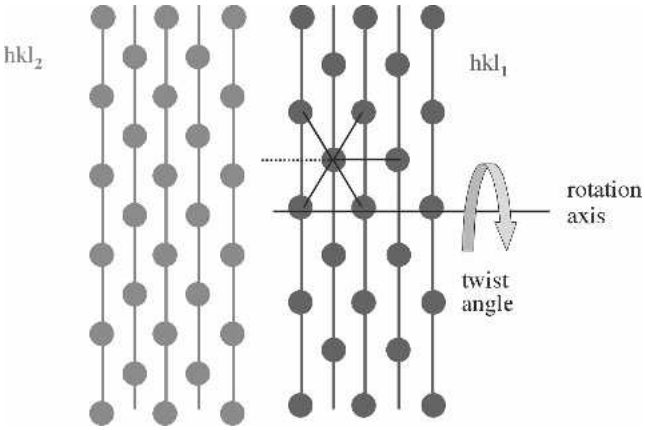

Fig. 2—Schematic of GB defined in the interface plane scheme showing nearest neighbor bonds of one atom (solid lines) and a dangling bond (dashed line).

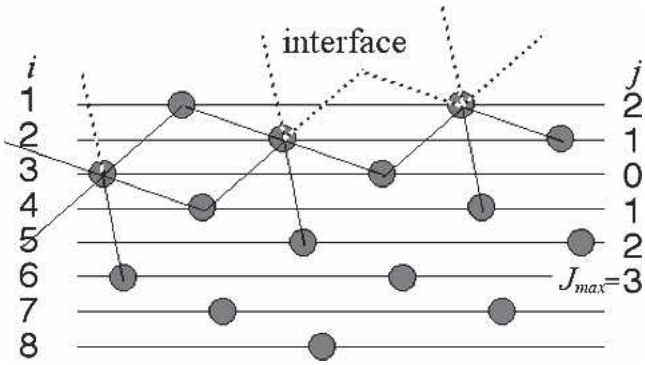

Fig. 3—Schematic of (*hkl*) surface showing nearest neighbor (nn) bonds (solid lines) and dangling nn bonds, as well as the relationship between the indices i and j for a case where $i = 3$ and $j = 3$.

ΔH^i_{seg} is the enthalpy of segregation to the ith plane, which includes both chemical and elastic energy terms.

For convenience, we also assume that the solute (B) corresponds to the segregating species. Although the solute is often the species that segregates to the interface, this is not invariably the case. However, in the event that the solvent is the segregating species, the enthalpy of segregation for the solute calculated by the model will turn out to be positive. From Eq. [30], it can be seen that a positive enthalpy will produce a lower atom fraction for B in the ith plane than in the bulk, thus correctly predicting solvent segregation for such a case.

We write the GB energy using an approach first employed to describe segregation to the free surface of a liquid.[46] In this approach, the GB energy is expressed as the interfacial excess grand potential, according to Eq. [21], with the interfacial excess free energy written in terms of the internal energy and the entropy, *i.e.*,

$$\gamma = e^s - Ts^s - \mu_A\Gamma_A - \mu_B\Gamma_B \qquad [31]$$

We now proceed to write each of the terms in Eq. [31], in the regular solution approximation, with the internal energy expressed in terms of nearest neighbor bonds. One important difference between GBs and crystalline surfaces, in the context of a nearest neighbor bond model, is that the relative locations of atoms across a GB are not compatible with nearest neighbor distances. At a two-component crystalline surface, the surface energy depends in part on the energy of the dangling bonds. In contrast, at a GB, a certain fraction of the dangling bonds of the atoms on one side of the GB will be reconnected to the atoms on the other side of the GB. Thus, a parameter, P, is used to represent the fraction of broken bonds at a surface that are reconnected to the other side of the GB when two surfaces are brought together to form a GB. The value of P depends on the Miller indices of the GB terminating planes, as well as the twist angle. A detailed derivation of that parameter has been given previously.[13]

We take each atom plane to contain n atoms per unit area (n will of course depend on the Miller indices (hkl) of the terminating plane), and for convenience, we write the internal energy for one side of the GB as follows:

$$\begin{aligned}
e^S \;=\; & \frac{nz^i}{2}\sum_{i=1}^{N+1}\left[(x^i)^2\varepsilon_{\text{BB}} + 2x^i(1-x^i)\varepsilon_{\text{AB}} + (1-x^i)^2\varepsilon_{\text{AA}}\right] - \Delta E^i_{el}x^i \\
& + \frac{n}{2}\sum_{i=2}^{J_{\max}}\sum_{j=1}^{i-1} z^j\left[x^ix^{i-j}\varepsilon_{\text{BB}} + x^i(1-x^{i-j})\varepsilon_{\text{AB}} + (1-x^i)x^{i-j}\varepsilon_{\text{AB}} + (1-x^i)(1-x^{i-j})\varepsilon_{\text{AA}}\right] \\
& + \frac{nP}{2}\sum_{i=1}^{J_{\max}}\sum_{j=i}^{J_{\max}} z^j\left[x^ix'\varepsilon_{\text{BB}} + x^i(1-x')\varepsilon_{\text{AB}} + (1-x^i)x'\varepsilon_{\text{AB}} + (1-x^i)(1-x')\varepsilon_{\text{AA}}\right] \\
& + \frac{n}{2}\sum_{i=1}^{J_{\max}}\sum_{j=1}^{J_{\max}} z^j\left[x^ix^{i+j}\varepsilon_{\text{BB}} + x^i(1-x^{i+j})\varepsilon_{\text{AB}} + (1-x^i)x^{i+j}\varepsilon_{\text{AB}} + (1-x^i)(1-x^{i+j})\varepsilon_{\text{AA}}\right] \\
& + \frac{n}{2}\sum_{i=J_{\max}+1}^{N+1}\sum_{j=1}^{J_{\max}} z^j\left[\begin{array}{l} x^ix^{i-j}\varepsilon_{\text{BB}} + x^i(1-x^{i-j})\varepsilon_{\text{AB}} + (1-x^i)x^{i-j}\varepsilon_{\text{AB}} + (1-x^i)(1-x^{i-j})\varepsilon_{\text{AA}} \\ + x^ix^{i+j}\varepsilon_{\text{BB}} + x^i(1-x^{i+j})\varepsilon_{\text{AB}} + (1-x^i)x^{i+j}\varepsilon_{\text{AB}} + (1-x^i)(1-x^{i+j})\varepsilon_{\text{AA}}\end{array}\right] \\
& - \frac{nz(N+1)}{2}\left[(x)^2\varepsilon_{\text{BB}} + 2x(1-x)\varepsilon_{\text{AB}} + (1-x)^2\varepsilon_{\text{AA}}\right]
\end{aligned} \qquad [32]$$

where the bond energies ε_{AA} and ε_{BB} are computed from the surface energies of the pure components and ε_{AB} from the regular solution constant of the AB binary alloy; ΔE^i_{el} is the bulk elastic energy of a solute atom that is relieved in layer i (and is computed as described in Reference 13); z^i is the number of nearest neighbors of an atom in the ith plane, which also lie in the ith plane, and z^j is the number of nearest neighbors of an atom in the ith plane, which lie in the jth plane (such that the total coordination of an atom is given by $z = z^i + 2\sum_{j=1}^{J_{\max}} z^j$), x' is a weighted average of the near-GB composition of the crystal on the other side of the boundary given by $x' = \sum_{i=1}^{J_{\max}}\sum_{j=i}^{J_{\max}} z^jx^i / \sum_{i=1}^{J_{\max}}\sum_{j=i}^{J_{\max}} z^j$, and N is the total number of planes, which have a composition different from the bulk. The value of N is taken to be several multiples of $J_{\max}$ (3 or 4 times $J_{\max}$ is generally sufficient to ensure that the Nth plane composition has essentially converged to that of the bulk). The first term in Eq. [32] represents the energy of in-plane bonds for all planes up to the $(N+1)$th; the second term calculates the energy of interface-directed bonds in planes $i = 2$ to $J_{\max}$ that are connected to atoms in planes closer to the interface; the third term accounts for (half of the) bonds that are connected to the other side of the GB; the fourth term accounts for the energy of bonds in the first $J_{\max}$ planes that point away from the interface; the fifth term represents the energy of out-of-plane bonds for planes $i = J_{\max} + 1$ to $N + 1$; and, finally, the sixth term subtracts the energy of $N + 1$ planes of bulk composition.

The surface excess entropy per unit area (for half the GB) is given by

$$\begin{aligned}
s^S = -nR\sum_{i=1}^{N}\big[&x^i\ \ln\ x^i + (1-x^i)\ \ln\ (1-x^i) \\
&-x\ \ln\ x - (1-x)\ \ln\ (1-x)\big]
\end{aligned} \qquad [33]$$

The chemical potentials of the components in a binary regular solution may be expressed as

$$\mu_{\text{A}} = \frac{z}{2}\left[2x^2\omega + \varepsilon_{\text{AA}}\right] + \text{R}T\ \ln\ (1-x) \qquad [34a]$$

and

$$\mu_B = \frac{z}{2}[2(1-x)^2\omega + \varepsilon_{BB}] + RT \ln x \quad [34b]$$

and the adsorptions of the two components (on one-half of the GB) are given by

$$\Gamma_A = n \sum_{i=1}^{N} (x - x^i) \quad [35a]$$

and

$$\Gamma_B = n \sum_{i=1}^{N} (x^i - x) \quad [35b]$$

Substituting Eqs. [32] through [35b] into Eq. [31] gives the energy of one side of the GB energy. By writing Eq. [31] for the second side of the GB, and adding it to the expression for the first side, one obtains the total GB energy. Minimizing the GB energy with respect to the atom fraction of each plane *i* yields expressions for the equilibrium atom fraction of solute in each atom plane. The expressions for the equilibrium atom fractions will have the form of Eq. [30], in which the heat of segregation of the *i*th atom plane is given by

$$\Delta H^i_{seg} = 2\omega \left[zx - z^i x^i - \sum_{j=1}^{J_{max}} z^j x^{i+j} - \sum_{j=1}^{i-1} z^j x^{i-j} - P \sum_{j=i}^{J_{max}} z^j x' - \frac{1}{2}(1-P) \sum_{j=i}^{J_{max}} z^j \right] - \frac{1}{2}(1-P)(\varepsilon_{BB} - \varepsilon_{AA}) \sum_{j=i}^{J_{max}} z^j - \Delta E^i_{el} \quad [36a]$$

for $i \leq J_{max}$, *i.e.*, planes with less than the bulk coordination, and by

$$\Delta H^i_{seg} = 2\omega \left[zx - z^i x^i - \sum_{j=1}^{J_{max}} z^j \left(x^{i+j} + x^{i-j} \right) \right] - \Delta E^i_{el} \quad [36b]$$

for the planes $N \geq i > J_{max}$. Equations [36a] and [36b] were actually derived by a different approach (Reference 13), but the resulting equilibrium plane compositions, obtained by substituting ΔH^i_{seg} into Eq. [30], were verified numerically to be minima of the interfacial energy, Eq. [31].

It should be noted that the equation for the composition of a given plane *i*, obtained by substituting ΔH^i_{seg} into Eq. [30], is transcendental and must be solved for the equilibrium plane composition by numerical methods. In addition, the equilibrium composition of a GB must be obtained iteratively. The compositions of all planes on both sides of the GB are initially set to the bulk composition, and the compositions on one side are computed. This allows a first approximation of x' for the first side to be calculated and used for the computation of compositions on the second side. The procedure is iterated until compositions on both sides converge.

Once the equilibrium plane compositions are known for both sides of the GB, they can be used in Eq. [31] to compute the GB energy. For the case of a symmetric boundary, where the terminating planes have the same value, $(hkl)_1$, the energy of the GB is just twice the energy of one side of the GB. For all other cases, the energies of the two sides are also just added. However, because the composition of one side depends on the composition of the other side through the term x', the near-boundary composition on one side with orientation $(hkl)_1$ will differ depending on the value of $(hkl)_2$ on the other side of the GB.

Unfortunately, there are no suitable experimental data sets on segregation to general GBs in fcc alloys that can be used to test the predictions of the preceding model. Nevertheless, it has been possible to test the model[13] against data sets for special GBs obtained by Udler and Seidman,[47,48] who conducted a series of consistent Monte Carlo simulations, in conjunction with embedded atom method (EAM) potentials,[49] on four alloys. These authors investigated the compositions of symmetric <100> twist GBs in Pt-1 at. pct Au, Au-1 at. pct Pt, Pt-3 at. pct Ni, and Ni-3 at. pct Pt. As an example, we show in Figure 4 a comparison between the predictions of the preceding model with the simulation results for the case of Pt-1 at. pct Au, in the form of a plot of adsorption *vs* twist angle. The figure shows good qualitative agreement, and reasonable quantitative agreement, between model and simulation results, both in terms of the dependence of adsorption on twist angle and on the effects of temperature on adsorption. Figure 4(b) displays a comparison of the plane-by-plane composition across the most highly segregated GB at a twist angle of ~43 deg. Here again, good agreement is obtained. Similar agreement was also found in the comparisons with the three other alloys for which simulations were performed,[13] thereby verifying that the model produces predictions that are compatible with the results of more sophisticated calculations.

C. *Application to Other Interfaces*

1. *General (hkl) surfaces*

The model for GBs can be particularized to several other cases of interest. For a general surface of orientation (hkl), the surface energy can be obtained from Eq. [31], with e^s written as in Eq. [32], but with the parameter *P* set to zero. Similarly, the equilibrium plane-by-plane near-surface compositions can be obtained by inserting the enthalpy of segregation of Eq. [36a], with $P = 0$, into Eq. [30]. These simplifications yield the expressions for the enthalpy of segregation of a free surface obtained previously by Steigerwald *et al.*:[42]

$$\Delta H^i_{seg} = 2\omega \left[zx - z^i x^i - \sum_{j=1}^{J_{max}} z^j x^{i+j} - \sum_{j=1}^{i-1} z^j x^{i-j} - \frac{1}{2} \sum_{j=i}^{J_{max}} z^j \right] - \frac{1}{2}(\varepsilon_{BB} - \varepsilon_{AA}) \sum_{j=i}^{J_{max}} z^j - \Delta E^i_{el} \quad [37]$$

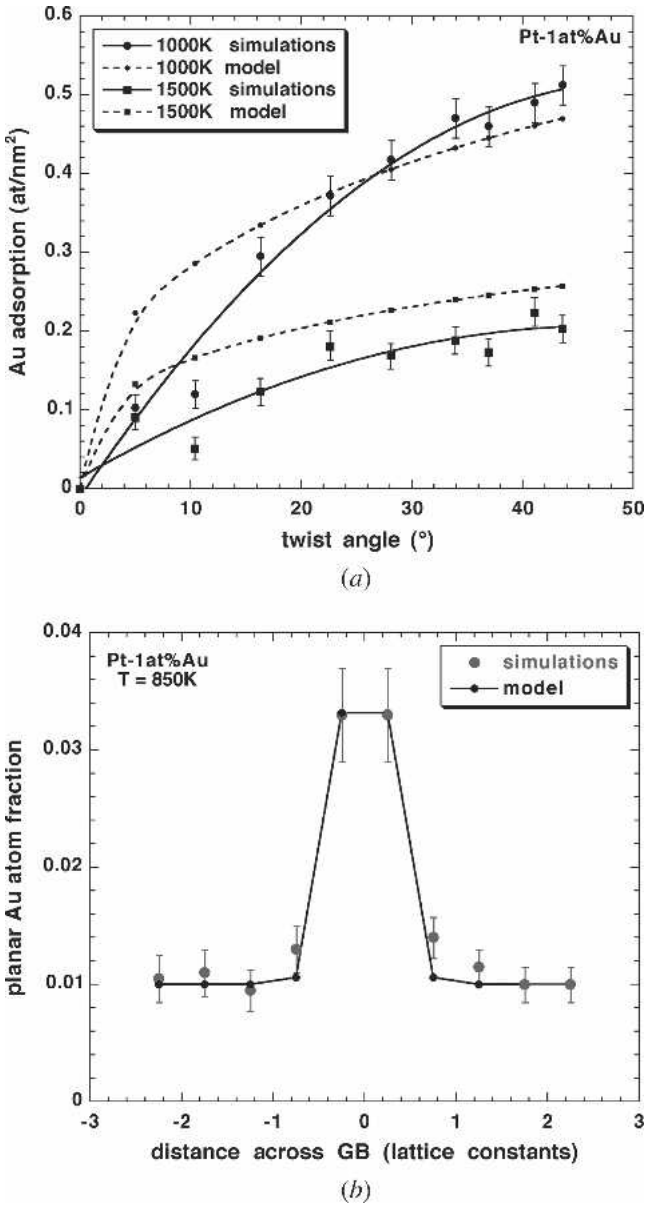

Fig. 4—Comparison between the GB segregation model[13] and the computer simulations of Udler and Seidman in Pt-1 at pct Au.[47,48] (*a*) Dependence of GB adsorption on twist angle for symmetric <100> twist GBs and (*b*) plane by plane composition for the GB at a twist angle of 43.6 deg.

for $i \leq J_{\max}$. Note that Eq. [36b] does not contain the parameter P and is therefore unchanged for surfaces from the form given previously in the case of a GB. In Eq. [37], the term $-1/2(\varepsilon_{BB} - \varepsilon_{AA}) \sum_{j=i}^{J_{\max}} z^j$, when summed over all atom planes for which $i \leq J_{\max}$, is just the molar surface energy difference of the pure components, $(\gamma_A - \gamma_B)\sigma$, which appears in the Defay and Prigogine monolayer expression (Eq. [26]) for the case $J_{\max} = 1$. In the GB model (Eq. [36a]), that term is multiplied by $(1 - P)$ to account for dangling bonds at a surface that are reconnected to the other side of the GB when two surfaces are joined to form a GB. Thus, rather than referring to that component of the chemical contribution to the enthalpy of segregation as the "surface energy" contribution, we will henceforth refer to it as the contribution that arises from the difference in the bond energies of the pure components.

Examples of results obtained for the surface energy and surface composition of (*hkl*) surfaces will be discussed in Section V.

2. *Liquid surfaces*

In the case of models aimed at describing segregation at liquid surfaces, it has been convenient to place the atoms of the liquid on an fcc lattice, in order to allow the use of a nearest neighbor model,[5,50,46] and to assume a coordination similar to that at a (111) surface. This is reasonable, since the coordination number in liquids is close to 12,[51] and the topmost surface atom layer of liquids is more highly ordered than the bulk of the liquid.[52] For simple surfaces, such as fcc (111), all of the out-of-plane bonds of a given atomic plane are connected to the adjacent atomic plane. Under those circumstances, the out-of-plane coordination number for a general plane (*hkl*), $\sum_{j=1}^{J_{\max}} z^j$, can simply be replaced by z^v (=3). In addition, the solute elastic strain energy term should be omitted. With these simplifications, the energy and near-surface composition of a liquid can be readily obtained.[46] We give here the relevant expressions for the equilibrium compositions:

$$RT \ln \frac{x^i}{1-x^i} = RT \ln \frac{x}{1-x} - \left\{ 2\omega[z^i(x-x^i) + z^v(2x - x^{i+1} - 0.5)] - \frac{z^v}{2}(\varepsilon_{BB} - \varepsilon_{AA}) \right\}; \quad i = 1 \qquad [38a]$$

$$RT \ln \frac{x^i}{1-x^i} = RT \ln \frac{x}{1-x} - \left\{ 2\omega\left[z^i\left(x-x^i\right) + z^v\left(2x - x^{i+1} - x^{i-1}\right)\right] \right\} \quad i > 1 \qquad [38b]$$

In the case of the liquid surfaces, ε_{AA} and ε_{BB} are computed from the pure liquid surface energies.

By way of historical perspective, it should be pointed out that Eqs. [38a] and [38b] are quite similar to those obtained by Williams and Nason,[53] for equilibrium near-surface composition, in a first attempt to account for multilayer segregation in alloys.

As an example, we compare in Figure 5 the predictions of the surface energy of liquid Ga-rich Ga-Pb alloys as a function of bulk Pb content calculated from this type of model, with experimental measurements of the surface energy by the sessile drop technique.[54] The figure shows a strong decrease of surface energy with increasing Pb atom fraction, as a result of Pb segregation to the liquid surface,[55] and indicates that there is good agreement between the model and the experimental results.

3. *Monolayer model*

Equation [38a] can readily be reduced to the monolayer model of Defay *et al.*[5] In that case, Eq. [38b] (for $i > 1$) is ignored, and the term x^{i+1} in Eq. [38a] is replaced by x, the bulk composition. It is also necessary to recognize that the term $-z^v(\varepsilon_{BB} - \varepsilon_{AA})/2$ is just the energy of the dangling

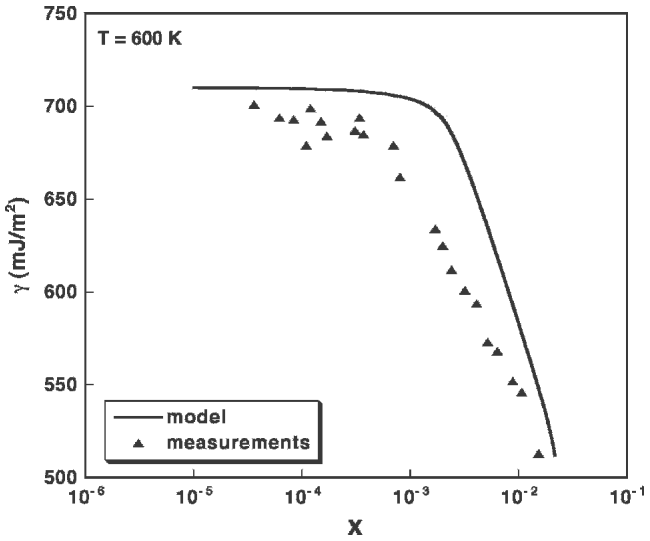

Fig. 5—Comparison of the surface energy of Ga-rich Ga-Pb alloys as a function of atom fraction Pb (x) calculated by Eq. [31][46] and measured by the sessile drop method[54]

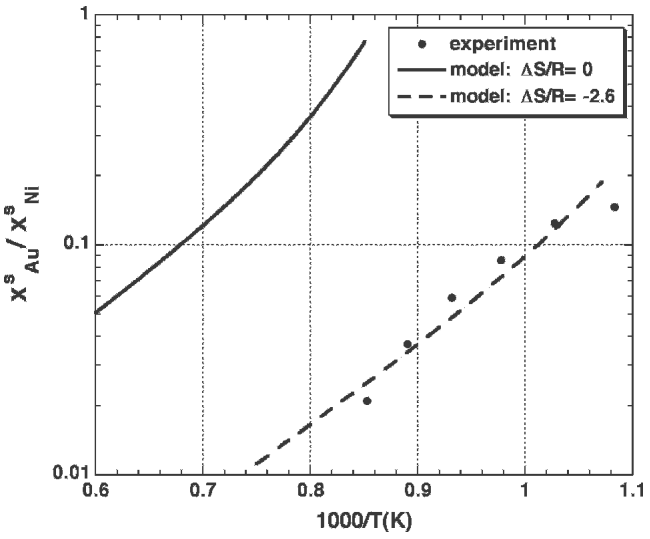

Fig. 6—Comparison of measured average surface segregation on a polycrystalline Ni-0.05 at pct Au alloy with monolayer model predictions for $\Delta S_{seg} = 0$ (regular solution) and with an added empirical entropy of segregation, $\Delta S_{seg}/R = -2.6$.[19]

bonds (for simple fcc surfaces such as (111) and (100)), and therefore represents the molar surface energy differen $(\gamma_B - \gamma_A)\sigma$. With these modifications, Eq. [38a] reduces to

$$RT \ln \frac{x^1}{1-x^1} = RT \ln \frac{x}{1-x} - \left\{(\gamma_B - \gamma_A)\sigma + \omega\left[z^i(x-x^1) + z^v\left(x-\tfrac{1}{2}\right)\right]\right\} \quad [39]$$

where x^1 is the composition of the monolayer, and leads to a heat of segregation that is identical to that of Defay *et al.*,[5] given in Eq. [26] for a liquid surface. For solids, where the solute elastic strain energy adds to the driving force for segregation, it is necessary to use expressions such as Eq. [27a] to compute the enthalpy of segregation, and hence the surface composition. As an example of the use of the monolayer model, we show in Figure 6 a comparison of its predictions with experimental surface segregation data obtained by Auger electron spectroscopy from the surface of an equilibrated Ni-0.05 at. pct Au polycrystalline alloy. The data are reported as effective surface compositions, x^1_{Au}/x^1_{Ni}, averaged over all surface orientations. These effective surface compositions are compared with model predictions for a (100) surface. Figure 6 also illustrates that the segregation enthalpy alone (*i.e.*, the use of a regular solution model) does not always yield good quantitative agreement with measurements. In general, quantitative agreement with experiment is improved by the addition of an excess entropy of segregation, as in Eq. [28]. However, it should be mentioned that this early approach to the interpretation of effective surface compositions is no longer recommended, as discussed in greater detail in Section V–B.

V. APPLICATIONS TO INTERFACIAL SEGREGATION

In this section, we exercise the various forms of the model described in Section IV to address several issues related to the anisotropy of interfacial segregation at GBs and surfaces. These include (a) the anisotropy of GB segregation, and its relation to GB energy; (b) the dependence of the composition of one side of a GB on the composition of the other side; (c) the difficulty of meaningful definitions of the segregation enthalpy and entropy; (d) the so-called compensation effect, which can lead to a crossover in plots of interfacial composition *vs* temperature for interfaces of different orientations; (e) the relative magnitudes of segregation at GBs and surfaces; and (f) the manner in which changes in the anisotropy of surface segregation with temperature can affect the temperature dependence of the equilibrium shape of crystals.

In most of the following illustrations of model trends, we use parameters obtained from embedded atom method potentials for the Pt-Au system,[49] and apply them to computations of segregation in Pt-Au alloys dilute in Au. This is the same choice of parameters as in the case of Figure 4, where model predictions were found to be in good agreement with computer simulations. The parameters include the pure component bond energies $\varepsilon_{PtPt} = -38{,}237$ J/mol and $\varepsilon_{AuAu} = -21{,}273$ J/mol (computed from the (100) surface energies), the regular solution constant $\omega = 562$ J/mol, the lattice constants $a_{Pt} = 0.392$ nm and $a_{Au} = 0.405$ nm, the bulk modulus $K_{Au} = 1.67$ ergs/cm^3, and the shear modulus $G_{Pt} = 0.68$ ergs/cm^3.[49] Calculations for Pt-Au are conducted for a bulk composition of $x = 0.01$. Occasionally, parameters corresponding to a hypothetical ideal solid solution will also be used, namely, $\varepsilon_{AA} = -46{,}347$ J/mol and $\varepsilon_{BB} = -23{,}173$ J/mol (corresponding to (100) surface energies of $\gamma_A = 2000$ mJ/m^2 and $\gamma_B = 1000$ mJ/m^2), and a lattice constant $a = 0.392$ nm (corresponding to Pt for convenience). Illustrations using other values will be specifically identified.

A. *Recent Results on GB Segregation Anisotropy*

It is well established that GB segregation is anisotropic.[7,56,57] However, most of the investigations of anisotropy

have tended to focus on "special" GBs. Thus, an adequate picture of the variation of GB segregation over the entire GB orientation space is still lacking. One of the more complete studies has reported measurements on 166 GB planes exposed by intergranular fracture in TiO_2-2 mol pct Nb_2O_5, and has addressed the manner in which Nb segregation varies with GB plane orientation over the standard stereographic triangle.[58] Because both the compositions and the orientations on both sides of each GB were determined, that study provided a first evaluation of the possible variation of GB composition over four of the five macroscopic parameters of the GB orientation space. However, before describing these results, we exercise the GB segregation model to investigate its predictions with respect to general trends in segregation anisotropy.

1. *GB model trends*

Figure 7 displays the composition at 1000 K of selected GBs in an fcc Pt-1 at. pct Au alloy. The figure shows the compositions of four GBs, all terminated by a (311) plane on one side, and four different (*hkl*) planes on the other, as a function of twist angle. The (311) plane lies on the (100)-(111) edge of the stereographic triangle. The other sides of the four GBs are terminated, respectively, by the (533), which also lies on the (100)-(111) edge, the (744) plane, which lies along the (110)-(111) edge, the (15 4 0) plane, which lies on the (100)-(110) edge, and the (321), which lies near the center of the triangle. Thus, the GB orientations are well distributed over the orientation space. Energy cusps that arise for these GBs at specific values of twist angle are indicated by arrows on the horizontal axis of the figure. Although the model correctly predicts the values of twist angle at which energy cusps are located, the depth of energy cusps is calculated rather crudely.[12,59] As a result, cusp values of the composition have been omitted. Nevertheless, Figure 7 indicates that the magnitude of compositional anisotropy of the GBs in dilute Pt-Au alloys ranges

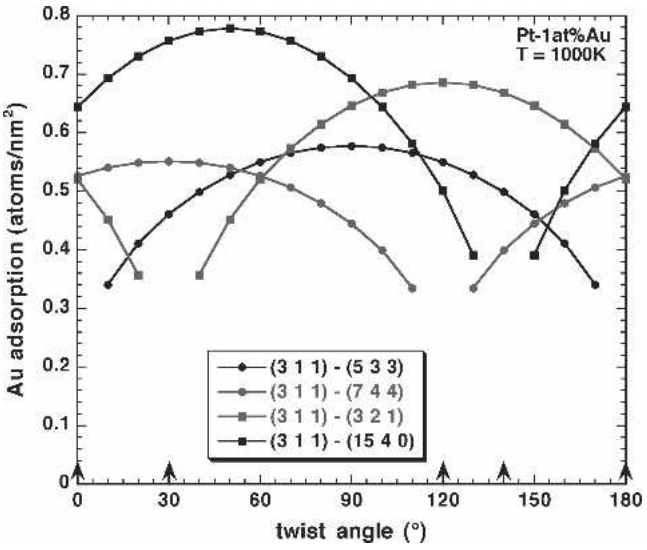

Fig. 7—Examples of model predictions for asymmetric twist GBs, as a function of twist angle, for a Pt-1 at. pct Au alloy at 1000 K. All GBs are terminated by a (311) plane on one side and by four different (*hkl*) planes on the other. Arrows indicate the location of cusps.[13]

over a factor of about 3 for the selected GBs. Of course, a larger anisotropy would be expected over the entire GB orientation space. Furthermore, the range of compositional anisotropy could be larger or smaller than in the specific case of the Pt-1 at. pct Au alloy used here for the purposes of illustration. Finally, it should be clear from the figures that variation of the fifth GB orientation parameter (twist angle) can also produce significant differences in GB segregation.

Displaying GB compositional information for the complete five-parameter space is impractical, as it requires a very large number of figures. In what follows, we therefore restrict the results displayed to a four-parameter space, in which the twist angle parameter is fixed at a value that corresponds to the maximum in GB composition for a given pair of terminating GB planes.

In Figure 8(a), we show the profiles across four GBs consisting of identical pairs of terminating planes, namely, (530)-(530), (511)-(511), (221)-(221), and (111)-(111). These profiles are all symmetric, as expected, and the figure shows that segregation is strongest for the (530)-(530) GB and weakest for the (111)-(111) GB. In Figure 8(b), the four GBs shown are comprised of a (530) terminating plane on the left-hand side (lhs), whereas the orientation on the rhs is varied through the sequence (530), (511), (221), and (111). The (530)-(530) boundary is of course identical in both figures and is only shown in Figure 8(b) for comparison. It can be seen in Figure 8(b) that the composition profile on the (530) side, *i.e.*, lhs of the GB, is dependent on the orientation of the rhs terminating plane. If the rhs plane is characterized by a weak segregation when it is present in a symmetric boundary, as indicated in Figure 8(a), then it also lowers the segregation profile on the (530) side of the GB in Figure 8(b). Similarly, the segregation on the more weakly segregated rhs terminating planes is raised when they are coupled with the strongly segregating (530) plane on the lhs. This provides evidence of the interaction of the segregant atoms across the GB, which comes about in the model from the terms containing the regular solution constant, ω. Thus, for the case of an ideal solution (*i.e.*, $\omega = 0$), the model predicts that the composition profile on one side of the GB would depend only on the orientation of the terminating plane on that side, and would be independent of the orientation of the plane on the other side of the GB. For nonzero values of ω, the degree of compositional interaction increases with increasing ω.

In order to illustrate the interaction across the GB over a broader range of the orientation parameters, we show in Figure 9(a) the variation over the standard stereographic triangle of the composition on each side of GBs terminated by identical (*hkl*) planes, and in Figure 9(b), the variation in composition of a terminating (111) plane when the other side of the GB varies over the stereographic triangle. This example is also for the case of the Pt-1 at. pct Au alloy, but for a temperature of 400 K. Figure 9(b) illustrates the effects seen in Figure 8, namely, that the composition of a (111) terminating plane is sensitive to the composition on the other side of the GB, and increases with increasing segregation on the other side. In Figure 9(a), the symmetric GBs display an anisotropy in composition that varies by a factor of 10 over the stereographic triangle, and Figure 9(b)

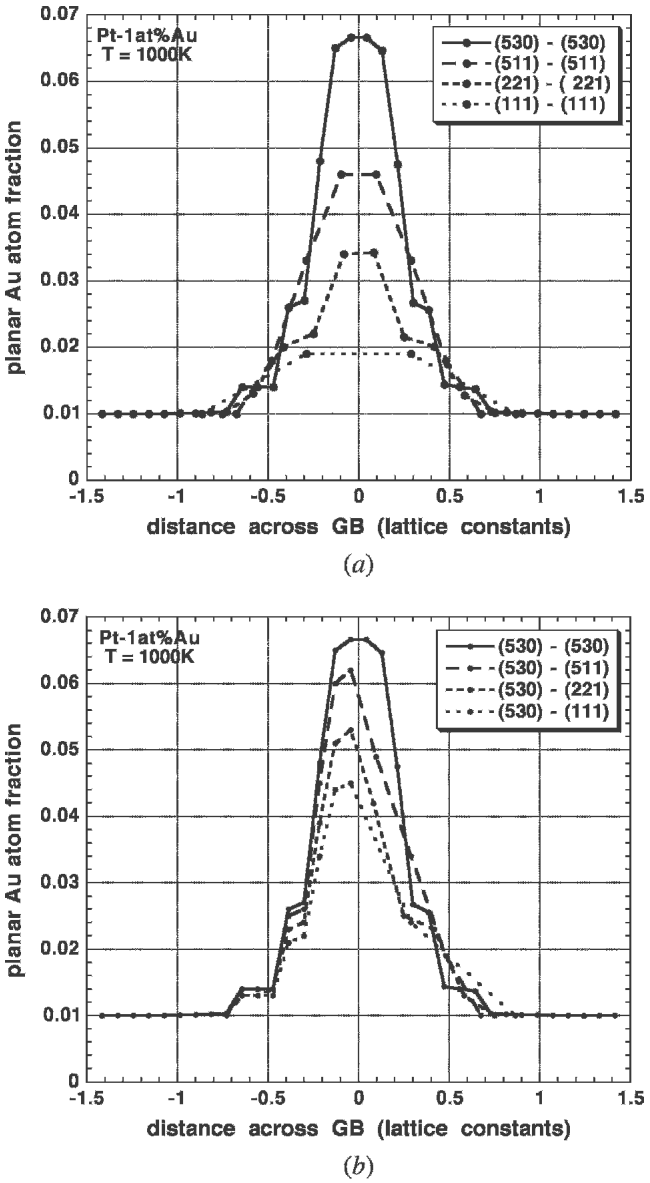

Fig. 8—Composition profiles across GBs in Pt-1 at pct Au at 1000 K. (*a*) GBs are terminated by identical pairs of planes, and (*b*) all GBs are terminated by a (530) plane on the left, and by (530), (511), (221), and (111), respectively, on the right.

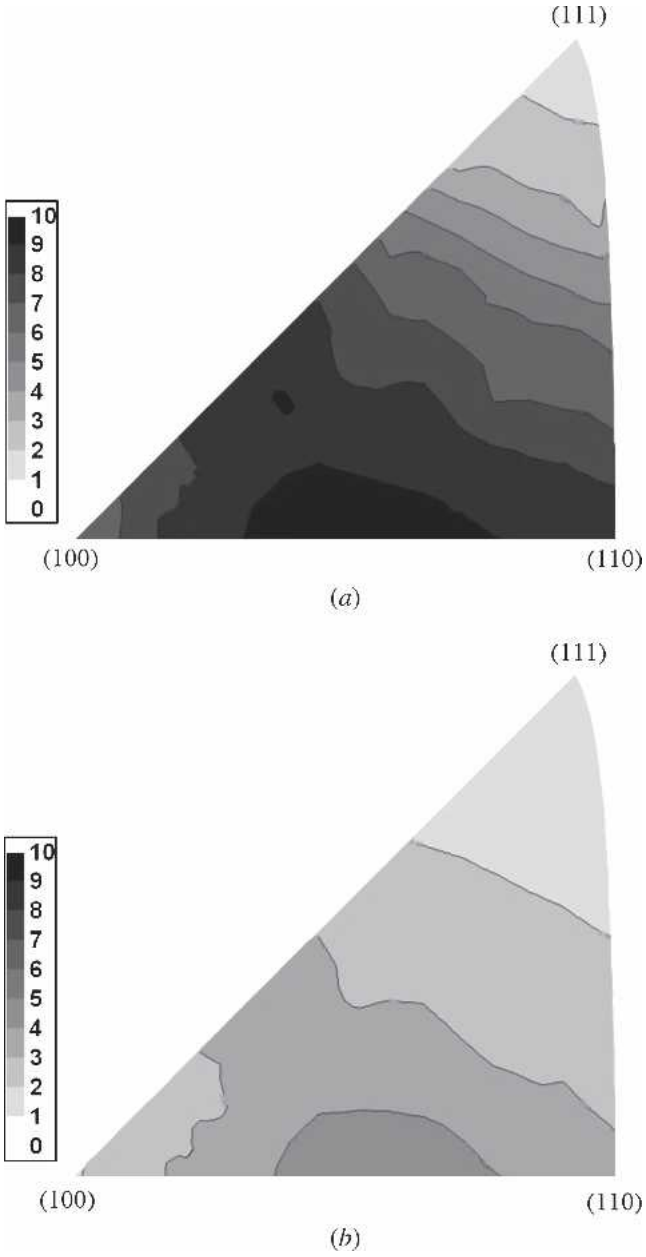

Fig. 9—Distribution of Au adsorption in Pt-1 at. pct Au at 400 K (*a*) on one side of the GB for GBs terminated on both sides by the same (*hkl*) orientation, and (*b*) on the (111) side of GBs terminated by the (111) orientation on one side and all possible orientations on the other side. The scale of the contour plots is in Au atoms/nm^2.

shows that the composition of the (111) side of GBs can range over a factor of 4 depending on the orientation of the terminating plane on the other side of the GB.

Finally, we show that there is a strong correlation between the level of segregation of a GB, and the energy of the GB in the pure solvent and in the segregated alloy. This is illustrated in Figure 10, which is a plot of adsorption *vs* GB energy either in pure Pt or in the equilibrated Pt-1 at. pct Au alloy at 400 K. The figure shows that segregation at these GBs is strongest in the case of high-energy boundaries and weakest in the case of low-energy boundaries. In addition, it shows the decrease in GB energy that results from segregation, which is most significant where the adsorption is largest, as expected from the Gibbs adsorption isotherm. However, a note of caution about the generality of this result should be injected here, in view of the possible reversal of the order of GB segregation with GB orientation (and energy) that can result from the so-called ''compensation effect.''[9] This issue will be discussed in more detail below in Section V–C.

2. *GB experimental results*

The experimental results used for comparison with the model predictions of the previous section were obtained in a study of Nb segregation to TiO_2 GBs in TiO_2-2 mol pct Nb_2O_5, after equilibration at ~1840 K.[58] These experimental results cannot be compared quantitatively to predictions

of the GB segregation model, as the model has not thus far been extended to metal oxide systems, where electrostatic effects need to be addressed. Nevertheless, a qualitative discussion of the results in light of general trends described previously can provide very useful insights.

Figure 11(a) summarizes the results of Nb GB segregation as a function of GB plane orientation, in which the GB normals are displayed in a stereographic triangle appropriate for tetragonal (rutile) TiO_2. The figure shows that the strongest segregation occurs for GB plane normals that lie along the (001)-(011) edge of the triangle, whereas the weakest segregation occurs for GB plane normals that lie close to the (110)-(010) edge of the triangle. Thus, there is a clear crystallographic separation of GB planes for which segregation is either strong or weak. The orientations corresponding to strong segregation are reproduced in Figure 11(b) (solid symbols) together with orientations of planes of the matching halves of those GBs (open symbols). Although the matching halves of GB planes displaying strong segregation are generally planes that show moderate segregation in Figure 11(a), they tend to fall in a region of orientation space that corresponds to strong segregation. Thus, in order for a GB plane to show relatively strong segregation, its matching half must also show relatively strong segregation. This is exactly the behavior that is expected from Figure 8, which shows that a given boundary plane will display strong segregation only if its matching half also displays relatively strong segregation.

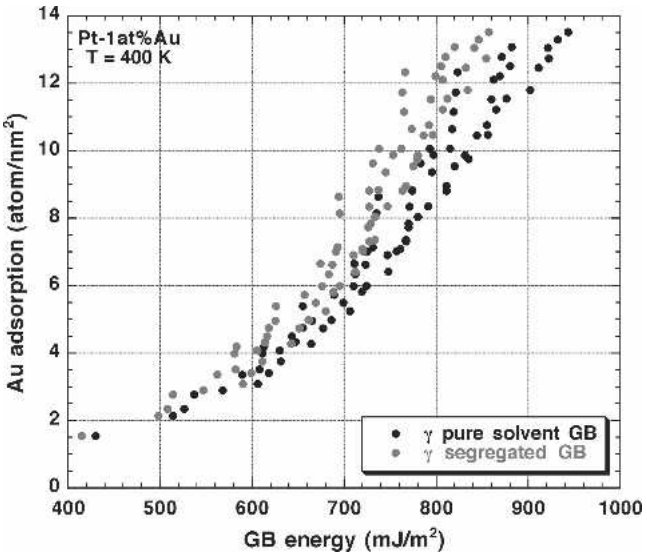

Fig. 10—Au adsorption at Pt-1 at. pct Au GBs at 400 K *vs* GB energy of pure Pt or of the segregated GB in the Pt-Au alloy. Calculation is for 78 different GBs with GB planes distributed over the stereographic triangle.

Figure 11(c) is a plot similar to 11(b), but for the case of GB planes exhibiting weak segregation. In this case, the matching planes of GBs displaying weak segregation also fall in a region of orientation space characterized by weaker segregation. This is also consistent with the qualitative trends predicted by the GB model in Figure 9, which shows that the composition of a (111) terminating plane is only low when segregation on the plane terminating the other side of the GB is also low.

Finally, we turn to a comparison between the prediction of stronger segregation to high-energy boundaries, shown in Figure 10, and the experimental results on Nb-doped TiO_2. As a prelude to this comparison, it is worthwhile to begin with a discussion of the relationship between GBs and surface energies in pure materials. Wolf[43,44,45] performed some important simulations aimed at understanding the anisotropy of GB energy. These simulations employed the interface plane scheme and showed that for a fixed pair of terminating surfaces, the GB energy was essentially constant over the entire range of twist angle, except for localized narrow cusps that occur at values of twist angle where the unit cell of the GB structure adopts a minimum size. In addition, Wolf found that the GB energy over the essentially constant ''plateau'' energy region was linearly related to the mean surface energy of the two terminating surfaces comprising the GB. The GB energy model that underlies the present GB segregation model[12,13] was also designed to reproduce this predicted trend. On the experimental side, Wolf's prediction of the relationship between mean surface energy and GB energy was verified by Saylor *et al.*,[10,11] in their measurements of the relative anisotropies of surface and GB energies in MgO. If we accept the result that GB energy scales with mean surface energy, then the results of Figure 10 imply that segregation on given GB planes

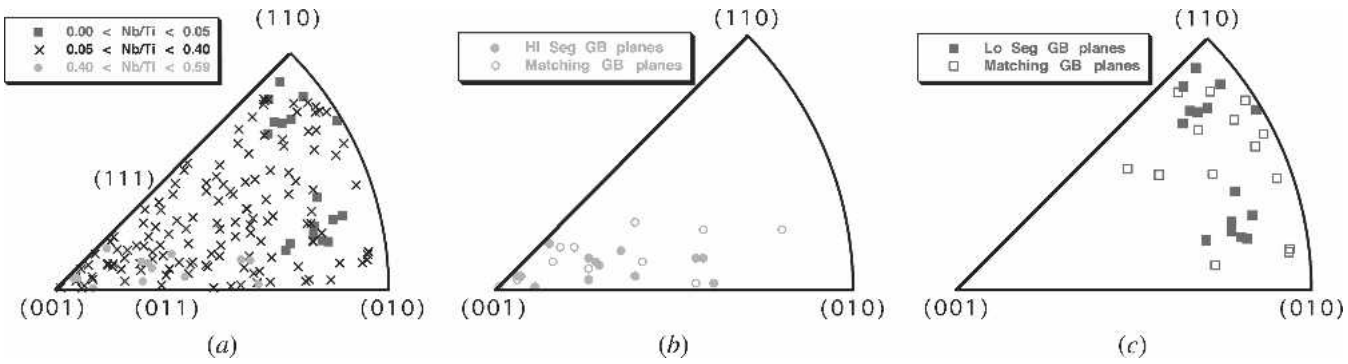

Fig. 11—(*a*) Orientation distribution of Nb segregation at TiO_2 GBs planes, displayed in the standard stereographic triangle for tetragonal rutile, and identifying orientations for which the Nb/Ti Auger peak ratio is high, moderate, or low. (*b*) GB plane orientations showing high levels of Nb segregation in (*a*) and the orientations of the matching planes on the other sides of the same GBs. (*c*) GB plane orientations showing low levels of Nb segregation in (*a*) and the orientations of the matching planes on the other sides of the same GBs.[58]

should scale approximately with the surface energy of that plane. In order to test these predictions in the case of Nb segregation to TiO_2 GBs, the anisotropy of surface energy of TiO_2 at 0 K was computed for all possible surface orientations,[8] based on first principles total energy calculations due to Ramamoorthy *et al.*[60] The results are shown in Figure 12. By comparing Figures 11(a) and 12, it can be seen that the GB plane orientations displaying high levels of Nb segregation in Figure 11(a) correspond to high-energy surfaces in pure TiO_2, and conversely, that low levels of Nb segregation are found on low-energy TiO_2 surfaces. These results are generally consistent with the predictions of the model shown in Figure 10, where high adsorption occurs on high-energy GBs, and *vice versa*.

B. *Effective Enthalpies and Entropies of Segregation*

There has been a great deal of confusion in the literature on the topic of the enthalpies and entropies of segregation. It is therefore worthwhile to address this topic here, in an effort to clarify the issues.

These thermodynamic parameters are generally extracted from measurements of interfacial composition as a function of temperature. Then, by assuming that the experimental results are described by means of a monolayer model, *i.e.*, by expressions such as Eq. [28], the enthalpy of segregation is obtained from the slope of $\ln \{x^s/(1-x^s)\}$ *vs* $1/T$ and the entropy from the intercept of the data at $1/T = 0$. However, there are questions related to the method by which x^s is measured, and also about the significance of the value extracted from such measurements.

For simplicity, we address this issue in the context of surface segregation. In general, even in the case of a surface where a single plane is lacking coordination (*e.g.*, fcc (111)), and for which the enthalpy of segregation may be expressed as in Eq. [27a], the enthalpy of segregation is a function of x^s, and is therefore dependent on temperature through the temperature dependence of x^s. This is because x^s approaches 1 in the limit $T \rightarrow 0$, and x^s approaches x as $T \rightarrow \infty$. In the temperature range where most of the temperature dependence takes place, the slope of $\ln \{x^s/(1-x^s)\}$ *vs* $1/T$ will yield an *effective* enthalpy of segregation, which is not equal to the value computed from Eq. [27a], and the intercept at infinite temperature will give a finite *effective* entropy of segregation, rather than the zero value consistent with the regular solution model.[20] The issue is even more complex in the case of a general (*hkl*) surface, where several near-surface planes lack coordination. Here, each near-surface atom plane will have a different characteristic enthalpy of segregation, and thus a different temperature dependence of composition. Such a "site dependence" of the enthalpy of segregation was pointed out a long time ago by White and Coghlan.[61] The net result is that the overall interfacial composition will no longer display a simple temperature dependence, with consequent effects on both the effective enthalpies and entropies of segregation.

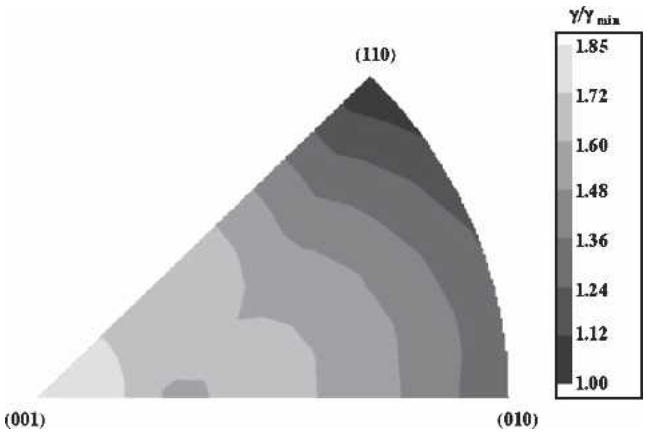

Fig. 12—Computed anisotropy of surface energy of TiO_2 (rutile) at 0 K.[8]

Matters are further complicated by the most common method of measuring the interfacial composition, namely, Auger electron spectroscopy (AES). The AES data are generally interpreted so as to yield an *effective* value of the quantity $x^s/(1-x^s)$, which is a convolution of the actual plane-by-plane composition and is given approximately by:

$$[x^s/(1-x^s)]^{\text{eff}} = \sum_{i=1}^{N} x^i \exp[-d(i-1)/\lambda] \Big/ \sum_{i=1}^{N} (1-x^i) \exp[-d(i-1)/\lambda] \qquad [40]$$

where x^i is the solute atom fraction in the ith atom plane, d is the interplanar spacing for the appropriate (*hkl*) surface, λ is a characteristic attenuation length related to the Auger electron emission process (which is typically a few tenths of a nanometer and can be different for the solute and solvent species), and N is a suitable number of planes that must be sufficiently large that the exponential attenuation makes contributions from deeper layers negligible. Equation [40] thus produces an effective interfacial composition, which is an average weighted by the exponential Auger signal attenuation term, $\exp[-d(i-1)/\lambda]$.

To illustrate these effects, we compare surface compositions calculated by the model, with what might be measured by AES for the (111) and (511) surfaces. The results shown in Figure 13(a) are obtained from the model for the case of the "standard" ideal solution described at the beginning of Section V. In this particularly simple case, there is no composition dependence of ΔH^i_{seg} (as this interaction only occurs for $\omega \neq 0$), and the only driving force for segregation arises from the difference between the bond energies of the pure solute and solvent. Figure 13(a) shows that a plot of $\ln \{x^i/(1-x^i)\}$ *vs* $1/T$, for each near-surface atom plane i, yields a straight line, as expected. The slope of each line is directly related to the appropriate ΔH^i_{seg}. To compute the trends that would be inferred from an AES measurement, we use Eq. [40], with $\lambda = 0.2$ nm, in order to give maximum weight to the near-surface atom planes. Those results are shown in Figure 13(b). Consider first the simple case of the (111) surface, in which only one atom plane differs in composition from the bulk (in the limit of an ideal solution). Even in this simple case, the effective value of the enthalpy of segregation, $\Delta H^{\text{eff}}_{\text{seg}}$, obtained from the slope of Figure 13(b), would be quite different from the ΔH^i_{seg} calculated by the model, with deviations becoming progressively more significant above $\ln \{x^s/(1-x^s)\}^{\text{eff}} \sim -1$ (*i.e.*, $x^s \sim 0.3$). For the case of the (511) surface, where

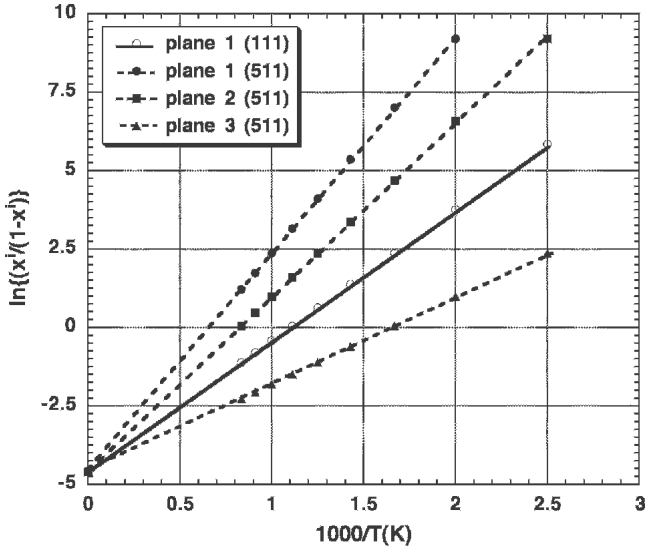

(*a*)

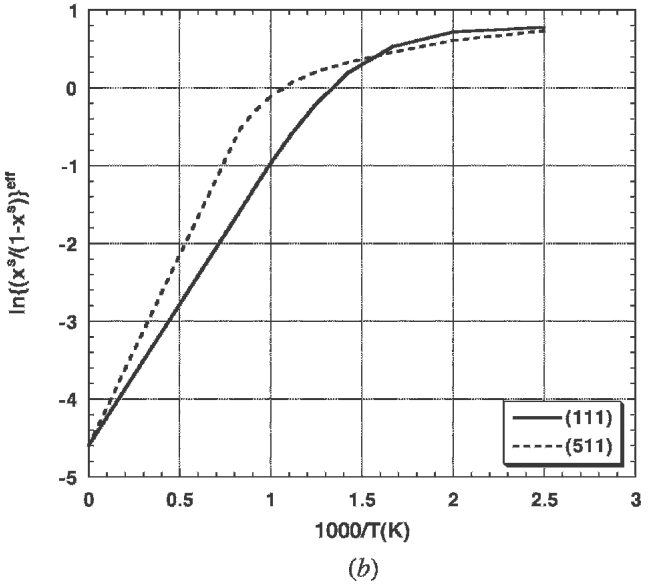

(*b*)

Fig. 13—(*a*) Calculated plane-by-plane variation of $\ln\{x^i/(1-x^i)\}$ *vs 1/T*, and (*b*) corresponding values of $\ln\{x^s/(1-x^s)\}^{\text{eff}}$ *vs 1/T*, which would be measured in an AES experiment, for (111) and (511) surfaces in a hypothetical ideal solution.

three planes differ in composition from the bulk, the value of $\Delta H^{\text{eff}}_{\text{seg}}$, obtained from the slope of the effective surface composition $\ln\{x^s/(1-x^s)\}^{\text{eff}}$ in Figure 13(b), bears no relation to the actual ΔH^i_{seg} calculated for each of the three atom planes.

The apparent asymptotic behavior of $\ln\{x^s/(1-x^s)\}^{\text{eff}}$ in Figure 13(b) comes about from the persistence of the AES signal from the substrate (generally the solvent component of the alloy), even when the surface layers are essentially saturated by the segregating component. However, even if this AES-specific problem could be avoided, it would be necessary to measure the changes in composition of individual atomic planes in the near-surface region as a function of temperature (as illustrated in Figure 13(a)) in order to extract physically meaningful enthalpies or entropies of segregation. Until such measurements are shown to be possible and reliable, the use of effective thermodynamic parameters to interpret measurements of interfacial segregation anisotropy should be avoided, as they lack any physical significance.

C. *Compensation Effect*

When the anisotropy of segregation has been studied, either at surfaces[42] or at GBs,[62] it has been found that the curves of interfacial composition *vs* temperature, for different orientations, can sometimes intersect close to a temperature that has been termed the compensation temperature. This phenomenon has been referred to as the compensation effect, because it has been interpreted as arising from a linear relationship between the enthalpy and the excess entropy of segregation. If such a relationship prevails, it would lead to the crossover of experimental curves at the compensating temperature, as described subsequently. It is worth recalling that a possible origin for the scaling of the excess entropy of segregation with the enthalpy of segregation was pointed out in Section III, in connection with Eq. [29b]. In addition, it is worth noting that similar compensation effects have also been reported for certain rate processes (*e.g.*, GB diffusion[63]).

In the context of equilibrium interfacial segregation, a compensation effect has been found when effective enthalpies ($\Delta H^{\text{eff}}_{\text{seg}}$) and entropies ($\Delta S^{\text{eff}}_{\text{seg}}$) of segregation have been extracted from relations such as

$$\left[\frac{x^S}{1-x^S}\right]^{\text{eff}} = \frac{x}{1-x}\,\exp\left\{\frac{\Delta S^{\text{eff}}_{\text{seg}}}{R}\right\}\,\exp\left\{-\frac{\Delta H^{\text{eff}}_{\text{seg}}}{\mathrm{R}T}\right\} \quad [41]$$

(*i.e.*, an "effective" version of Eq. [28]) together with values of $\ln[x^s/(1-x^s)]^{\text{eff}}$ obtained from AES experiments *via* Eq. [40]. If one supposes that the effective enthalpies and entropies of segregation for different orientations are linearly related as follows:

$$\Delta S^{\text{eff}}_{\text{seg}} = \Delta H^{\text{eff}}_{\text{seg}} \Big/ T_{\text{comp}} + C \quad [42a]$$

and

$$\Delta G^{\text{eff}}_{\text{seg}} = \Delta H^{\text{eff}}_{\text{seg}} - T\Delta S^{\text{eff}}_{\text{seg}} \quad [42b]$$

where T_{comp} is the compensation temperature and C is a constant, then $\Delta G^{\text{eff}}_{\text{seg}}$ *vs* T for all possible orientations will intersect at T_{comp}, and $\Delta G^{\text{eff}}_{\text{seg}}$ will adopt a value of $-C$ at T_{comp}, for all possible choices satisfying Eq. [42a]. However, in view of the lack of physical meaning of these effective parameters, as discussed in Section V–B, this argument does not provide a useful rationale for the origin of the compensation effect.

To illustrate that the compensation phenomenon is consistent with the predictions of regular solution type models, we have calculated the adsorption for several surface orientations in the limit of our standard ideal solution. The ideal solution approximation is used here, because it has been found, by exercising the model, that the compensation effect essentially arises from the difference between the

bond energies of the pure components, and not from the interatomic interaction terms that depend on ω, nor from the elastic strain energy contribution to the driving force. The latter contributions to the segregation driving force may modify the temperature at which two orientations have the same value of ΔG_{seg}^{eff}, but do not, on their own, produce the compensation effect. The plane-by-plane compositions shown in these illustrations have been obtained by using the enthalpies of Eq. [37], and these have been inserted into Eq. [35b] to obtain the total solute adsorption.

The results are displayed in Figure 14 in the form of a plot of adsorption *vs* temperature for seven surface orientations distributed around the stereographic triangle. The figure shows that most of the curves intersect over a relatively limited temperature range in the vicinity of 800 K to give an approximately equal surface composition for the various orientations. Only the (100) orientation seems to behave somewhat differently from the others. Apart from the anomaly of the (100) orientation, an apparent ''compensation effect'' is present, even though the enthalpy of segregation is finite, but the excess entropy of segregation is zero for these ideal solution calculations. Thus, the interpretation of the intersection of composition curves at a particular temperature is clearly unrelated to a compensation between the excess entropies and enthalpies of segregation that might arise from some linear relationship between these thermodynamic parameters.

In order to investigate the origin of the common surface composition at about 800 K, we have plotted the plane-by-plane contributions for the (111) and (211) surface orientations, in the ideal solution limit, in Figure 15. The (111) orientation has only one atom plane that differs from the bulk composition in the ideal solution limit. This plane is characterized by three dangling bonds. In contrast, the (211) orientation has five, three, and two dangling bonds in the first, second, and third atom planes, respectively. The planar site density is 15/nm^2 for a (111) plane, but only 5.3/nm^2 for a (211) plane (for an assumed lattice constant of 0.392 nm corresponding to Pt). Figure 15 shows that the first (211) surface plane saturates in segregant at ~800 K, *i.e.*, at a higher temperature than the others, because it has the highest number of dangling bonds, and therefore the strongest driving force for segregation. It is followed by the second (211) surface plane with three dangling bonds, which saturates at ~500 K, and the third plane with two dangling bonds that saturates at ~300 K. The (111) surface plane saturates at the same temperature as the second (211) plane, since it has the same number of dangling bonds. However, because of the stronger segregation to the first plane of the (211) surface, total adsorption on (211) exceeds that of the (111) surface plane at high temperature. As one proceeds to lower temperatures, total adsorption on the (211) surface is eventually overtaken by total adsorption on the (111), at about 800 K, due to the ~3 times larger number of atom (or adsorption) sites per (111) plane than per (211) plane. The intersection in total adsorption at ~800 K thus reflects a complex interplay between the numbers of dangling bonds in each segregated plane, the numbers of planes that can contain excess solute, as well as the number of atom sites per plane. These three variables are listed in Table I for all of the surface orientations used in the illustration in Figure 14.

One possible reason for the anomalous behavior of the (100) orientation can be seen in Table I, which shows that the single plane with broken bonds in the case of the (100) surface orientation has four dangling bonds, whereas the average number of broken bonds per atom plane for all other orientations is much closer to three. Table I also shows that the parameters responsible for crossover have a significant range of values; thus, it is not surprising that crossovers in total adsorption can occur for all orientations. However, the origin of an almost universal crossover temperature of

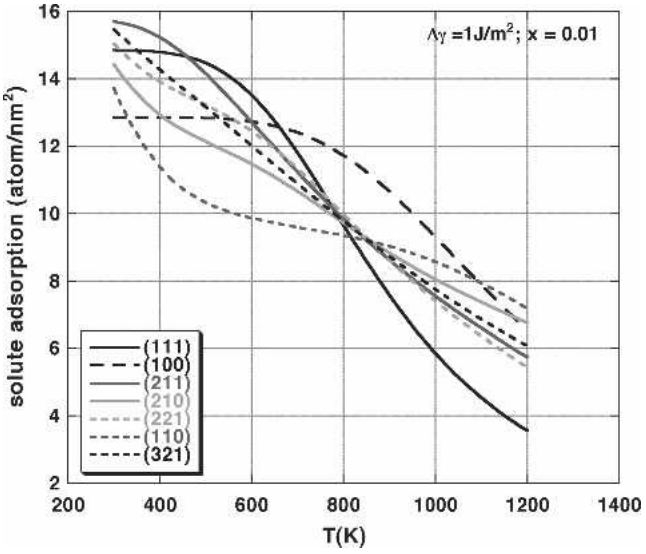

Fig. 14—Solute adsorption *vs* temperature for seven different surface orientations, for the hypothetical ideal solution of Fig. 13, illustrating the intersection of most adsorption curves near 800 K (the lattice constant for the solution has been taken as 0.392 nm).

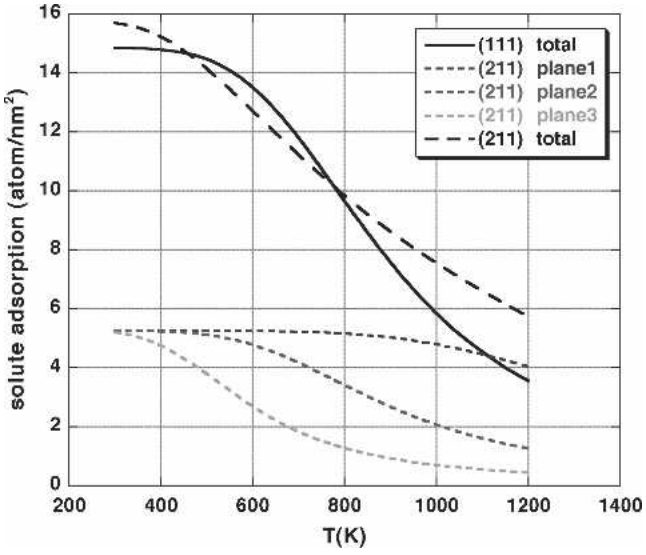

Fig. 15—Solute adsorption as a function of temperature for the (111) and (211) surface orientations of the hypothetical ideal solution of Fig. 13, showing plane-by-plane adsorption contributions for the (211) surface. (The lattice constant for the solution has been taken as 0.392 nm.)

Table I. Variables Associated with the Different Surface Orientations of Figure 14

Surface Orientation	Broken Bonds in the *ith* Plane					Average Number of Broken Bonds/Plane	Adsorption Sites/Plane (nm^{-2})	Total Number of Adsorption Sites (nm^{-2})
	i = 1	i = 2	i = 3	i = 4	i = 5			
(111)	3					3	15	15
(100)	4					4	13	13
(211)	5	3	2			3.3	5.3	15.9
(210)	6	3	1			3.3	5.8	17.4
(221)	5	3	3	1		3	4.3	17.3
(110)	5	1				3	9.2	18.4
(321)	6	4	3	2	1	3.2	3.5	17.5

~800 K is still not obvious. Furthermore, it should be noted that as temperature is decreased below ~800 K, Figure 14 shows that additional intersections of the adsorption curves can occur. A second intersection point is also shown, for example, between the adsorptions on (111) and (211) in Figure 15 at ~500 K. The second intersection shown in Figure 15, as well as some of those in Figure 14, are simply the result of different numbers of adsorption sites for the various surface orientations. Table I indicates that the (111) surface plane has 15 adsorption sites/nm^2, whereas the three (211) surface planes have a total of ~15.9 adsorption sites/nm^2. Therefore, in the limit of low temperatures, the (211) surface will necessarily saturate at a higher total adsorption than the (111) surface, thereby leading to the second intersection. One important conclusion from this analysis is that the intersection of adsorption curves for different orientations is not due to a compensation effect resulting from a relationship between the excess entropy and enthalpy of segregation. As a result, we prefer to refer to this phenomenon as the crossover effect.

Setting aside the (100) orientation anomaly of Figure 14, it can be seen that above the crossover temperature of ~800 K, the adsorption is lowest for the lowest-energy (111) surface, but highest on that surface below the intersection temperature. Indeed, at temperatures above the crossover temperature, there is a reasonable correlation between increasing adsorption and increasing surface energy. This is illustrated in Figure 16(a), in the ideal solution limit, for more than 30 surface orientations distributed over the stereographic triangle. The few orientations that tend to lie off the general trend are low index surfaces (noted on the figure). The trends displayed in Figure 16(a) are similar to those previously shown for Pt-1 at. pct Au GBs in Figure 10. Because of the relatively small number of orientations displayed in Figure 14, the adsorption below the crossover temperature might be interpreted as indicating a systematic trend of lower adsorption at higher energy surfaces. However, the relation between adsorption and surface energy is not as simple below the crossover temperature. This is illustrated in Figure 16(b) at a temperature of 600 K, for the same set of surface orientations as Figure 16(a). This figure shows that adsorption can vary significantly without much change in surface energy. In the limit of very low temperatures, where adsorption sites will tend to be saturated with segregant, the last column of Table I indicates that adsorption anisotropy will tend to disappear.

As mentioned previously, it has been shown experimentally[62] that the crossover phenomenon described here for surfaces also occurs at GBs. However, comparable calculations performed with the GB model, using realistic values

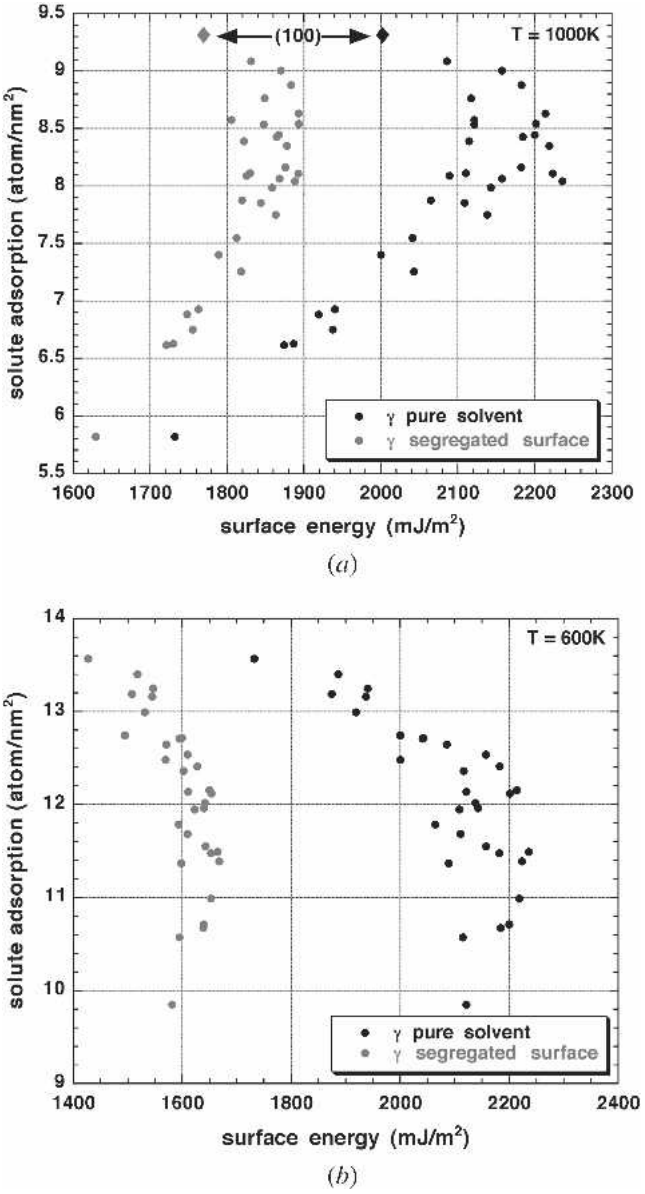

Fig. 16—Variation of solute adsorption with surface energy for the hypothetical ideal solution of Fig. 13. Both the pure solvent and segregated surface energies are shown: (*a*) at 1000 K and (*b*) at 600 K.

of the difference between the pure component bond energies, do not display the crossover effect. This is because the contribution of the pure component bond energy difference to the driving force for segregation is much smaller in the case of GBs than in the case of free surfaces, as a result of the much smaller number of broken bonds at a GB. Most of the bonds that are broken at a free surface tend to be reconnected when two surfaces are joined to form a GB, thereby reducing the magnitude of the pure component bond energy contribution that yields the crossover effect. This result might be an artifact of the GB model, and may therefore be worthy of further investigation.

Finally, it is worth noting that the existence of an almost fixed crossover temperature for most orientations, illustrated in this section for the case of an ideal solution, does not occur for all values of the segregation parameters. An example where the intersections of the adsorption curves *vs* temperature, for different orientations, occur over a broad range of temperatures will be shown below in Section E. Thus, the significance, if any, of the crossover phenomenon is unclear.

D. *Comparison between Surface and GB Segregation*

The enthalpies of segregation for GBs (Eqs. [36a] and [36b]) and surfaces (Eq. [37]) in metallic alloys contain the same types of terms. For both types of interface, the enthalpies include terms arising from the difference in bond energies of the two pure components, which have been referred to as a surface energy contribution; terms that arise from the regular solution constant, ω, which have been referred to as alloy interaction contributions and which also depend on the interfacial composition; and terms that depend on the solute elastic strain energy. The terms related to the pure component bond energies reflect the total numbers of dangling bonds for the two interfaces. Since the numbers of dangling bonds (per interface atom) at a GB are considerably smaller than at a free surface, the driving force for segregation arising from these terms will be much smaller at a GB than at a surface. The alloy interaction terms enhance segregation when ω is positive (*i.e*., in systems with a tendency to cluster), and their contribution to the driving force is magnified by an increase in the number of neighbors of an interface atom. Thus, since the coordination of an atom at a GB is larger than that at a free surface, these terms can enhance the driving force for segregation at a GB in relation to a surface. The solute strain energy terms reflect the energy decrease that results from exchanging a solute atom in the bulk with a solvent atom at the interface. This is likely to be greater at a free surface than at a GB, because the atomic environment of a solute atom at a free surface is more open (*i.e*., less constrained) than it is at a GB. However, when this hypothesis was tested by allowing for an adjustable parameter in the comparison of model predictions for GBs with the results of computer simulations,[13] it was found that there is essentially no adjustment needed to correct the solute strain energy term for GBs in relation to free surfaces. Thus, in the present model, the absolute weight of solute elastic strain energy contributions is the same for GB and surface segregation (although the relative weight may be different).

This discussion implies that surface segregation will generally be stronger at a free surface than at a GB when the enthalpy of segregation is dominated by differences between the bond energies of the pure solute and solvent. Conversely, segregation could be stronger at a GB than at a surface if the enthalpy of segregation is dominated by the terms in ω. Examples of these two cases are shown in Figures 17(a) and (b). Figure 17(a) shows a comparison between segregation at a (321)-(321) GB and a (321) surface, using Pt-1 at pct Au as the example, where the enthalpy is dominated by bond energy differences. The adsorption at the surface is higher over most of the temperature range. However, even in this case, GB segregation catches up to surface segregation as interface saturation occurs at sufficiently low temperatures. This intersection of the segregation curves results from the fact that the number of adsorption sites at the GB is twice as large as the number of surface adsorption sites. In Figure 17(b), the model parameters have been changed by eliminating the bond energy difference and the solute strain energy contributions, and by increasing the value of ω from 0.562 kJ/mol for Pt-Au to 2kJ/mol. Since this higher value of ω leads to a lower bulk solubility, it has also been necessary to lower the bulk solute content from 1 at. pct in Pt-Au to 0.05 at. pct. Figure 17(b) shows that with this change in parameters, the GB adsorption is always higher than the surface adsorption, and is in fact more than twice that at the surface, thereby ensuring that the stronger GB segregation does not merely reflect the higher number of GB adsorption sites.

The preceding example serves to illustrate that surface segregation need not always be stronger than GB segregation, although that has been the more common experimental observation when surface and GB segregation have been compared.[64–67] Some of the work in this area has compared the segregation behavior of surfaces and GBs in the context of three or more component alloys, where the behavior may be more complex due to possible solute-solute interactions at the interface.

E. *Surface Segregation Anisotropy and the Equilibrium Shape of Alloy Crystals*

Two principal experimental approaches have been used to measure surface energy anisotropy. The first has involved studies of interfacial equilibrium at the intersection of either twin boundaries[68] or general GBs[69] with surfaces. The second approach has relied on direct observations of the shapes of small crystals, since the anisotropy of surface energy is related to the equilibrium crystal shape (ECS) by the Wulff construction.[70,71] Whereas the ECS of pure fcc metals has been the subject of significant study, *e.g*., in the case of Pb,[72] Au,[73,74,75] and Cu,[76] there has been relatively little comparable work performed on fcc alloys. Some examples of fcc alloys where data have been obtained on the effects of adsorption on surface energy anisotropy include Cu-O,[77] Cu-Bi,[78] and Pb-Bi-Ni.[79] The work on Cu-O falls outside the purview of the present model approach, since Cu-O alloys cannot easily be described within that framework. However, all of the experimental observations display some common trends that are worthy of discussion in light of model predictions.

In all of the experimental studies of alloys cited previously, solute adsorption is quite strong, and the surface energy anisotropy of the pure solvent is increased as a result

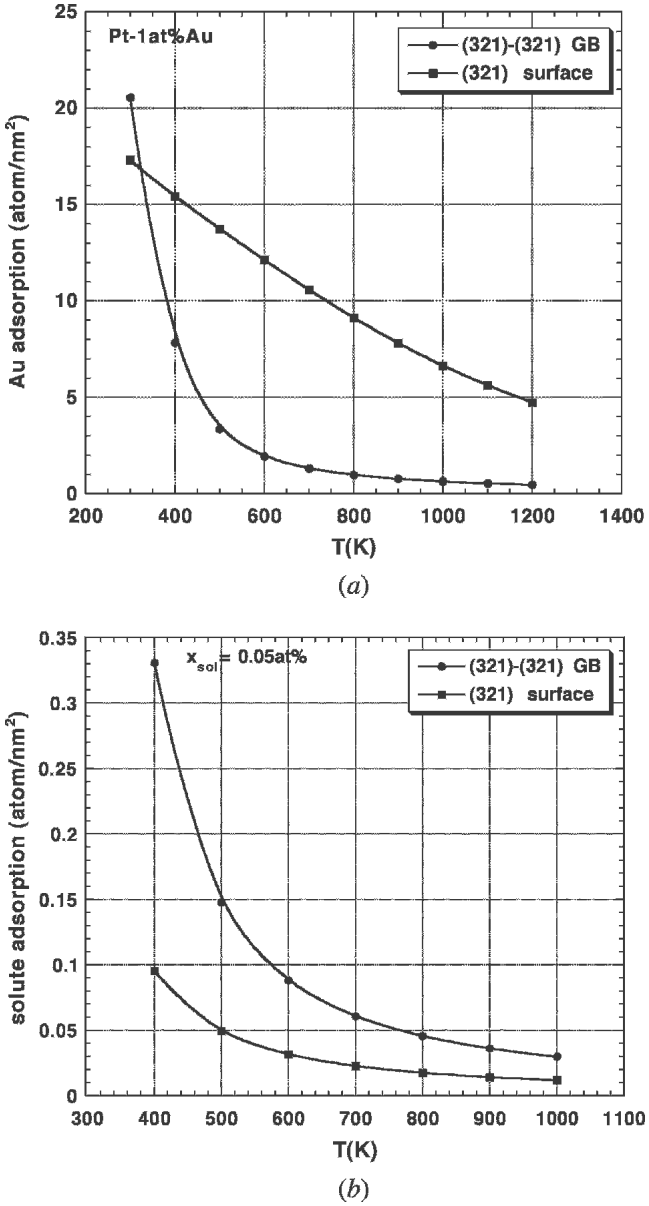

Fig. 17—Comparison of adsorption *vs* temperature (*a*) for a (321)-(321) GB and a (321) surface in the Pt-1 at pct Au alloy, and (*b*) for a hypothetical alloy with no bond energy difference between the pure components, a regular solution constant of $\omega = 2$ kJ/mol, and a bulk solute concentration of $x = 0.05$ at pct.

of the adsorption. This may appear to contradict the results displayed in Figure 10 for Pt-Au GBs and in Figures 16 for the surfaces of an ideal solution. In both those cases, the ratio of maximum to minimum interfacial energy is larger for the pure solvent interfaces than for the segregated interfaces. However, the behavior shown in those examples is not general, and probably stems from the relatively weak segregation in those cases. In Figure 18, we use the example of a more strongly segregating alloy system, namely, Ni-Au, to illustrate that surface energy anisotropy can be increased by solute segregation. The model parameters used for Ni-Au alloys are as follows: $\varepsilon_{NiNi} = -36{,}258$ J/mol, $\varepsilon_{AuAu} = -26{,}352$ J/mol, $\omega = 2487$ J/mol, $a_{Ni} = 0.352$ nm, $a_{Au} = 0.408$ nm, $K_{Au} = 1.77$ ergs/cm^3, and $G_{Ni} = 0.77$ ergs/cm^3.[42]

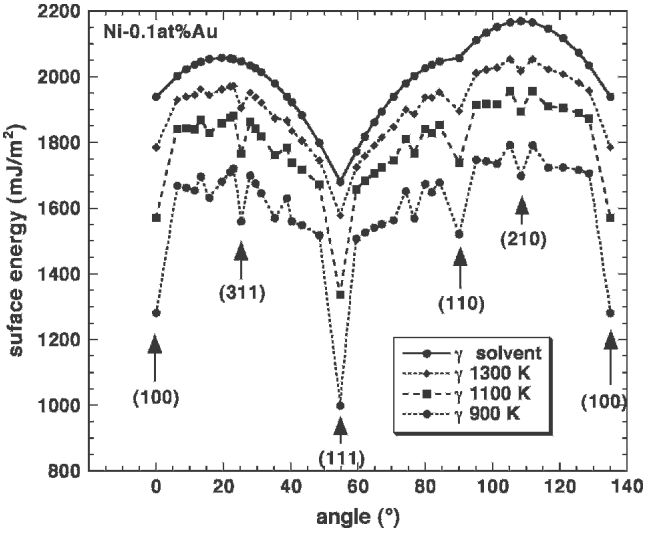

Fig. 18—Surface energy variation with orientation around the edge of the stereographic triangle. Curves are shown for the pure solvent and for a Ni-0.1 at. pct Au alloy at three temperatures.

Figure 18 shows the calculated variation in surface energy for the pure Ni solvent, as well as that for a Ni-0.1 at. pct Au alloy at three temperatures, as the surface orientation is varied around the edges of the standard stereographic triangle (*i.e.*, from (100) to (111) to (110) and finally back to (100)). As can be seen, the anisotropy of surface energy is significantly increased by Au segregation to the Ni-alloy surface. Thus, by comparing Figure 18 to Figures 10 and 16, we find that interfacial energy anisotropy can either be decreased or increased, depending on the values of the parameters that determine the driving force for segregation.

Before proceeding to a further discussion of the consequences of adsorption shown in Figure 18, it is useful to begin with a discussion of the surface energy anisotropy of pure fcc metals, and in particular of the occurrence of facets on the ECS. The existence of cusps in the orientation dependence of interfacial energy is a necessary, but not a sufficient, condition for the appearance of facets on the ECS.[71] In order for a facet to occur on the ECS, not only must a cusp in surface energy be present, but the cusp must also penetrate the inner envelope of Wulff planes that define the ECS. Thus, the anisotropy of surface energy shown in the upper curve of Figure 18 (labeled as γ solvent) implies that pure fcc metals can at most display facets only at {111}, {100}, and {110} orientations. In pure Pb and Au, experiments have shown[72–75] that the ECS consists predominantly of curved surfaces, with small facets at {111} and {100} orientations. However, measurements of the ECS can only be performed at high temperatures, in order to avoid prohibitively long equilibration times. As a result, shallow cusps that may exist in the orientation dependence of surface energy at low temperatures can disappear at higher temperatures due to entropy effects, by so-called faceting-roughening transitions. For example, although {110} facets were not seen on the ECS of pure Pb,[72] subsequent crystal growth experiments showed that facets at {110} orientations do eventually become stable at temperatures

below those where the ECS measurements were performed.[80] In addition, studies of the ECS of pure Cu[76] at 1240 K have shown that it also consists of predominantly curved surfaces with small facets. However, in this case, facets occur not only at {111} and {100}, but also at {110} orientations. Thus, the prediction by the model of cusps at {111}, {100}, and {110} in pure fcc metals is consistent with available measurements. It should also be noted that the present model predictions for the surface energy of pure crystals does not account for temperature (*i.e.*, entropy) effects and cannot therefore provide predictions of faceting-roughening transitions. This also means that the anisotropy of pure fcc metals calculated by the model corresponds to a temperature of 0 K, and is therefore typically larger than that measured experimentally. Finally, since the model is for a "generic" fcc metal, it is unable to identify differences in behavior among different fcc metals. In light of all these limitations of the model, the qualitative agreement with data on pure fcc metals is therefore comforting.

We return now to the results of Figure 18 relating to solute adsorption. The most important result in this context is that the anisotropic adsorption and the related changes in surface energy anisotropy lead to the development of new cusps at several orientations, notably at (311) and (210) orientations. In the case of experiments on Pb containing Bi and Ni additions, the ECS was studied as a function of temperature.[79] At the highest temperatures, just below the melting point, the ECS of a Pb-5 at. pct Bi-0.04 at. pct Ni alloy was found to be similar to that of pure Pb and to display small facets only at {111} and {100} orientations. Upon cooling, the first change in anisotropy manifested itself as an increase in {111}-facet size. This result is generally consistent with Figure 18, where the most significant surface energy decrease occurs for the (111) orientation. Upon further cooling, the first new facet to appear on the Pb alloy ECS had an orientation somewhere between (311) and (411) (which could not precisely be identified). This is similar to the results of Figure 18, which shows the development of a new cusp at (311). We will return subsequently to a discussion of the factors that could lead to small differences in facet orientation. The next new facet to form on the Pb alloy ECS, upon further temperature decrease, was the {110}, which also displays increasing cusp depth with decreasing temperature in Figure 18. A photomicrograph of a Pb-5 at. pct Bi-0.04 at. pct Ni crystal after appearance of the {110} facets is shown in Figure 19(a).

Measurements of the ECS of Bi-saturated Cu were only performed at a temperature of 1223 K.[78] In this case, the ECS was completely faceted (*i.e.*, no curved surfaces were present) and displayed only {111}, {100}, {110}, and {320} facets, as shown in the partially equilibrated "negative" crystal displayed in Figure 19(b). It is interesting to note that the "generic" segregated fcc alloy of Figure 18 displays a new cusp due to segregation at the (210) orientation, not far from (320). One reason that the model may not predict the precise orientations at which new cusps are expected to form probably stems from its neglect of possible surface reconstruction effects. For example, in the case of Bi on Cu(100), the adsorbed Bi atoms can order into c(2 × 2), c(9√2 × √2)R45 deg, and p(10 × 10) structures[81,82] with increasing Bi coverage. These significant structural

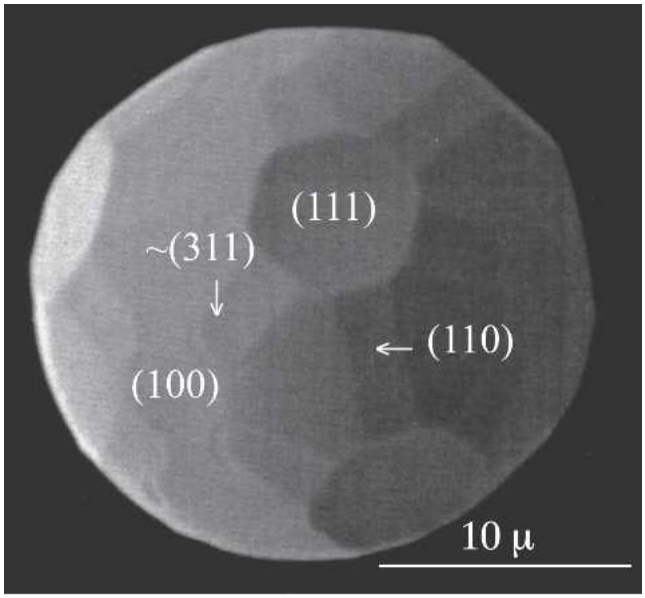

(*a*)

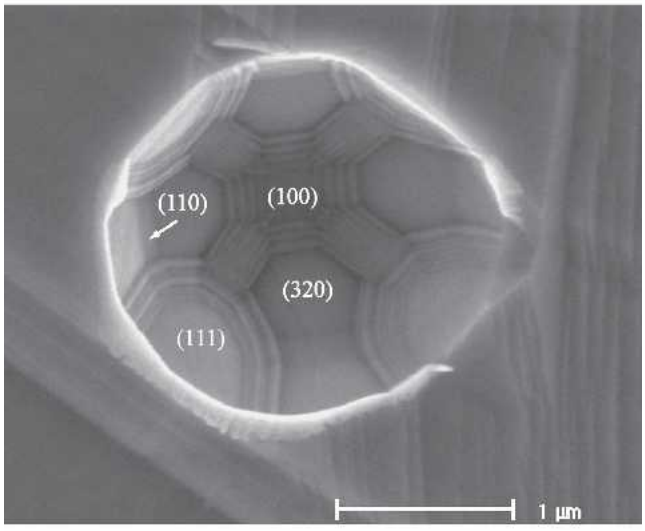

(*b*)

Fig. 19—(*a*) ECS of Pb-5 at. pct Bi-0.04 at. pct Ni equilibrated at 498 K, displaying facets at {111}, {100}, {110}, and in the vicinity of {311} orientations, together with curved surfaces;[79] and (*b*) nearly equilibrated GB pore in Bi-saturated Cu at 1223 K, displaying facets at {111}, {100}, {110}, and {320} orientations, separated by microfaceted regions of the same orientations.[78]

changes with increasing adsorption are presumably tied to the large size mismatch between Bi and the underlying Cu substrate. Thus, the level of adsorption on a surface of any given orientation will depend not only on the parameters included in the segregation model, but also on the ease with which mismatching segregated solute atoms can be accommodated on the template provided by the surface structure of the solvent (substrate). These structural effects may lead to surface configurations that differ in both adsorption and energy from those predicted by a model that does not account for interface reconstruction effects.

In our discussion of the so-called compensation effect in Section C, we saw that crossovers can occur in the dependence

of adsorption on temperature for surfaces of different orientation, as shown in Figure 14 for an ideal solution alloy. Figure 20 is a plot similar to Figure 14, but for the case of the Ni-0.1 at. pct Au alloy. One conclusion that should be noted from Figure 20 is that it does not display a common temperature for which all surface orientations show approximately equal adsorption. This makes the point that the crossover phenomenon is not necessarily a general feature of the anisotropy of segregation.

In Figure 21, we plot the surface energy ratios of several pairs of surface orientations shown in Figure 20, as a function of temperature, in order to illustrate the interesting finding that *for any pair of orientations, the ratio of the surface energies displays a minimum at the temperature corresponding to the crossover in adsorption for those two surface orientations*. While we have not been able thus far to demonstrate this result analytically, starting from an appropriate form of Eq. [32], it appears to be quite general, based on numerical evaluations of the type shown in Figure 21. Thus, although Figure 20 indicates an overall increase in surface energy anisotropy with increasing segregation, the behavior of any pair of orientations that undergo a crossover in adsorption will be such as to show first a decreasing anisotropy, and then an increasing anisotropy, as temperature is decreased and the overall level segregation increases. These results show clearly that it is not possible to make any generalizations on whether segregation will tend to increase or decrease the anisotropy of interfacial energy.

Last, we display in Figure 22 the predicted effects of segregation on the ECS of the Ni-Au alloy used in the illustrations of this section. The equilibrium crystal shapes shown in the figure have been computed by means of Wulffman software[83] from the computed energies of the segregated Ni-Au surfaces at various temperatures; the shapes are viewed along a <110> direction. If we consider first the relative sizes of the {100} and {111} facets, we see that the ratio $\gamma_{(100)}/\gamma_{(111)}$ is high at the lowest temperature (*i.e.*, relatively small {100} facets), reaches a minimum around 1250 K, and then increases again, although not very significantly. If we consider the {110} facets, they are absent at the lowest temperature, indicating that the energy cusp at that orientation does not penetrate the inner envelope of Wulff planes. However, these facets make their appearance on the ECS between 1200 and 1250 K, increase in size with increasing temperature up to 1300 K, and then decrease in size, although they do not completely disappear even at 1700 K. The facet shape shown at 1300 K in Figure 22 is quite similar to that observed on the ECS of a Pb-5 at. pct Bi-0.08 at. pct Ni alloy (*i.e.*, an alloy with double the Ni concentration of that shown in Figure 19(a)) at 523 K, as illustrated in Figure 23. The only important difference between the ECS of this Pb alloy and the Ni-Au alloy at 1300 K is that the Pb alloy still displays some curved surfaces; *i.e.*, it is not completely faceted. These minor differences are most likely due to neglect of excess and surface entropy effects in the surface segregation model.

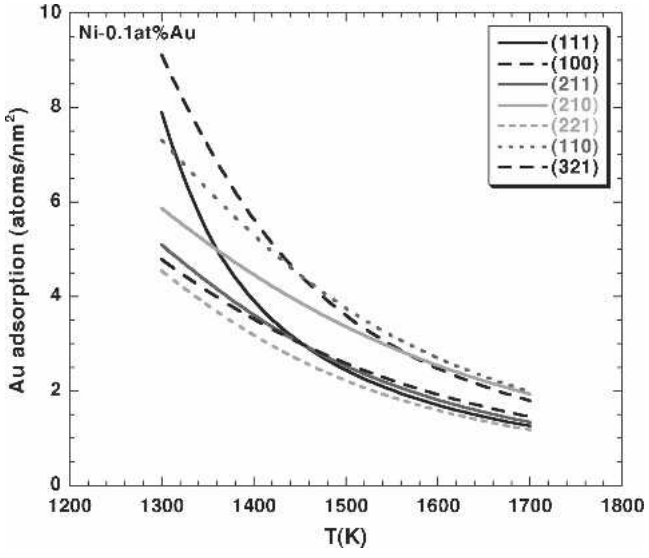

Fig. 20—Adsorption *vs* temperature for seven different surface orientations calculated for a Ni-0.1 at. pct Au alloy.

The preceding results indicate that it would be interesting to extend the model to interphase boundaries, as this would provide a means of investigating the equilibrium shape of precipitates of one phase in another. Such an extension would also allow the evaluation of segregation effects at interphase boundaries that might allow tailoring of alloying additions to produce precipitates of desirable shapes.

VI. SUMMARY AND CONCLUSIONS

Analytical models for probing the anisotropy of interfacial segregation in the case of GBs and free surfaces have been presented. The most general case described is a GB segregation model, based on the regular solution approximation, which accounts for the five macroscopic parameters of the GB orientation space. It is shown that most of the previous regular solution-type models of segregation can be derived from the GB segregation model, by appropriate simplifications. In addition, the relationship between the models and the Gibbsian thermodynamics of adsorption is clarified.

The GB segregation model has been exercised to identify general trends in GB segregation anisotropy. It is shown that GB segregation is sensitive to all five of the macroscopic GB orientation parameters. In addition, the composition profile of the segregated species across a GB is shown to depend on the crystallographic orientations of the two planes terminating the GB. In the case of regular solutions, where there is a finite interaction between the atomic species across the GB, the composition on one side of a GB terminated by a given crystallographic plane depends on crystallographic orientation of the plane terminating the other side of the GB. This model prediction is supported by experimental evidence.

The significance of experimentally derived effective enthalpies and entropies of segregation has been analyzed. It is shown that these thermodynamic parameters lack physical significance for any realistic situation where some atoms of the segregated species are located beyond the first atomic plane parallel to the interface. It is therefore concluded that the use of these parameters for interpretation of data are best avoided.

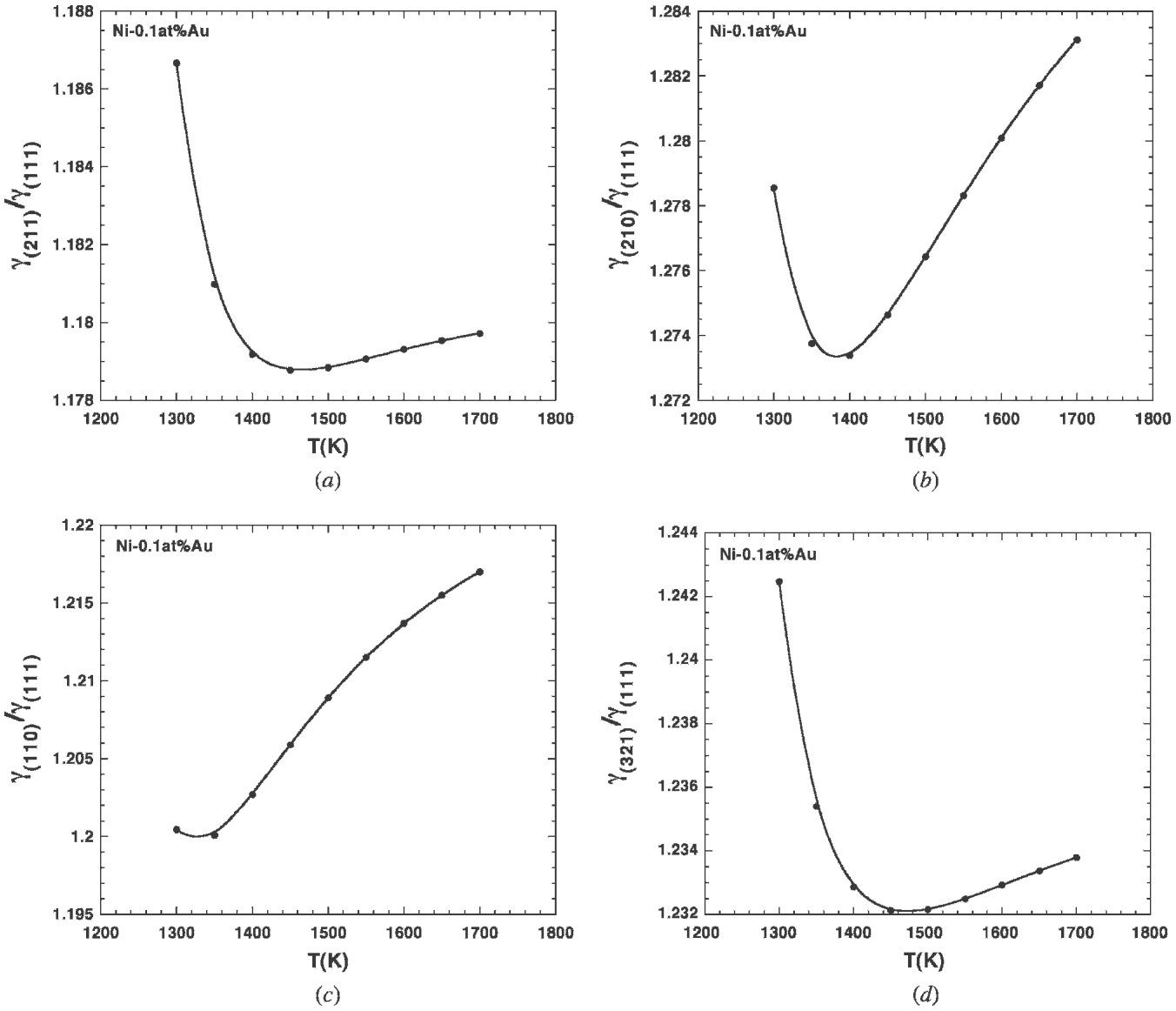

Fig. 21—Surface energy ratios of various pairs of orientations in Ni-0.1 at. pct Au, as a function of temperature: (*a*) $\gamma_{(211)}/\gamma_{(111)}$, (*b*) $\gamma_{(210)}/\gamma_{(111)}$, (*c*) $\gamma_{(110)}/\gamma_{(111)}$, and (*d*) $\gamma_{(321)}/\gamma_{(111)}$.

The so-called compensation effect has been analyzed. It is shown that previous interpretations of this effect as arising from a linear relationship between the effective enthalpies and entropies of segregation are incorrect, as the effect occurs even in ideal solutions where the effective entropy is set to zero. The compensation effect in these ideal solutions seems to arise from a complex interplay between the numbers of dangling bonds in each segregated plane, the numbers of planes that can contain excess solute, as well as the number of atom sites per plane. In the case of regular solutions, the compensation effect is not always present; thus, its significance, if any, is unclear.

A comparison has been made between GB and surface segregation. Although adsorption is generally expected to be higher at surfaces than at GBs, it is possible for GB adsorption to be higher than that at a surface if the interatomic interaction contributions to the driving force for segregation dominate other contributions.

The anisotropy of surface segregation and its effects on the anisotropy of surface energy have been investigated, in an effort to ascertain whether segregation tends to increase or decrease interfacial energy anisotropy. The conclusion reached is that it is not possible to generalize, as segregation can either increase or decrease the interfacial energy anisotropy. In addition, the following interesting finding has emerged from the results: for any pair of orientations, the ratio of the surface energies displays a minimum at the temperature corresponding to the crossover in adsorption for those two surface orientations. Finally, the effects of surface segregation on equilibrium crystal shape have been addressed. The general trends predicted by the model are found to be in agreement with previous experimental results.

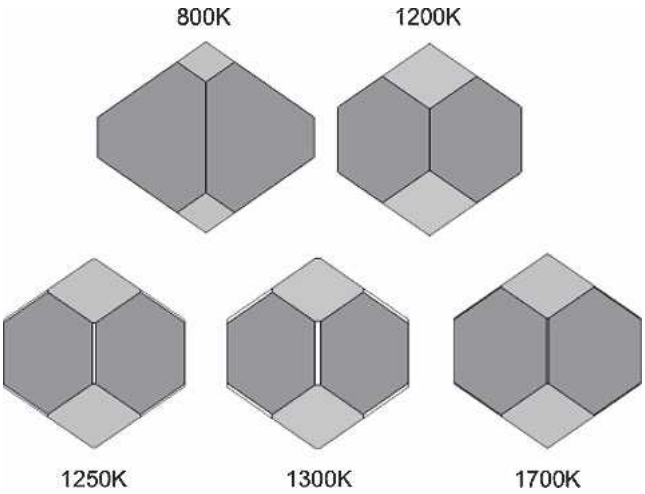

Fig. 22—Equilibrium crystal shapes of Ni-0.1 at. pct Au at various temperatures, computed by means of the Wulffman software.[83]

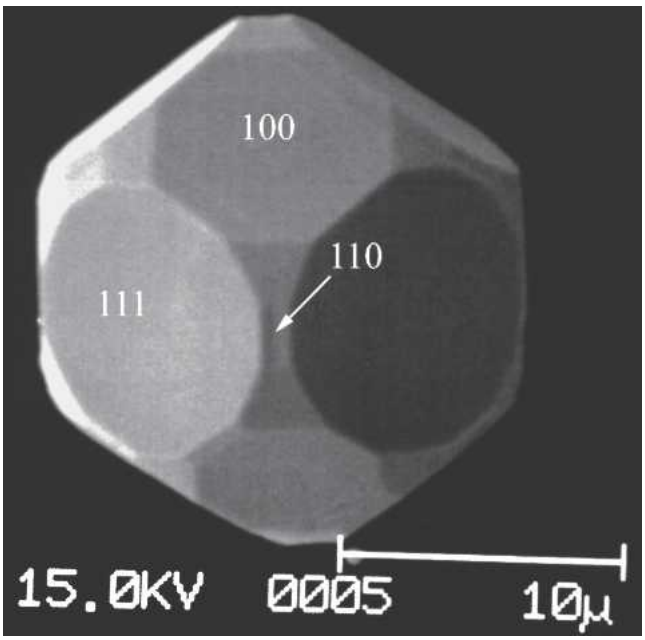

Fig. 23—Crystal of Pb-5 at. pct Bi-0.08 at. pct Ni equilibrated for 13 h at 523 K.

ACKNOWLEDGMENT

One of the authors (PW) acknowledges with thanks the support of this research by the MRSEC Program of the National Science Foundation under Award No. DMR-0520425.

REFERENCES

1. J.W. Gibbs: *The Scientific Papers of J. Willard Gibbs*, Dover. New York, NY, 1961, vol. 1, pp. 219-331.
2. R.H. Fowler and E.A. Guggenheim: *Statistical Thermodynamics*, Macmillan, New York, NY, 1939, pp. 429-40.
3. S. Ono and S. Kondo: in *Encyclopedia of Physics*, S. Flugge, ed., Springer, Berlin, 1960, vol. X, pp. 134-277.
4. D. McLean: *Grain Boundaries in Metals*, Oxford Press, London, 1957, pp. 116-22.
5. R. Defay, I. Prigogine, A. Bellmans, and D.H. Everett: *Surface Tension and Adsorption*, Wiley, New York, NY, 1966, pp. 158-97.
6. G.S. Rohrer, D.M. Saylor, B. El Dasher, B. Adams, A.D. Rollett, and P. Wynblatt: *Z Metallkd.*, 2004, vol. 95, pp. 197-214.
7. D.N. Seidman: *Annu. Rev. Mater. Res.*, 2002, vol. 32, pp. 235-69.
8. Y. Pang and P. Wynblatt: *J. Am. Ceram. Soc.*, 2006, vol. 89, pp. 666-71.
9. P. Wynblatt, Z. Shi, Y. Pang, and D. Chatain: *Z. Metallkd.*, 2005, vol. 96, pp. 1142-46.
10. D.M. Saylor, A. Morawiec, and G.S. Rohrer: *J. Am. Ceram. Soc.*, 2002, vol. 85, pp. 3081-83.
11. D.M. Saylor, A. Morawiec, and G.S. Rohrer: *Acta Mater.*, 2003, vol. 51, pp. 3675-86.
12. P. Wynblatt and M. Takashima: *Interface Sci.*, 2001, vol. 9, pp. 265-73.
13. P. Wynblatt and Z. Shi: *J. Mater. Sci.*, 2005, vol. 40, pp. 2765-73.
14. W.W. Mullins: *Metal Surfaces*, ASM, Cleveland, OH, 1963, p. 17-66.
15. J.P. Hirth: *Structure and Properties of Metal Surfaces*, Honda Memorial Series in Materials Science No. 1, Maruzen Co. Ltd., Tokyo, 1973, pp. 10-33.
16. E.D. Hondros and M.P. Seah: *Metall. Trans. A*, 1977, vol. 8A, pp. 1363-71.
17. J. Langmuir: *J. Am. Chem. Soc.*, 1916, vol. 38, pp. 2221-95.
18. J.J. Burton and E.S. Machlin: *Phys. Rev. Lett.*, 1976, vol. 37, pp. 1433-36.
19. P. Wynblatt and R.C. Ku: *Surf. Sci.*, 1977, vol. 65, pp. 511-31.
20. P. Wynblatt and R.C. Ku: in *Interfacial Segregation*, W.C. Johnson and J.M. Blakely, eds., ASM, Metals Park, OH, 1979, pp. 115-36.
21. J. Friedel: *Adv. Phys.,* 1954, vol. 3, pp. 446-507.
22. Y.W. Lee and H.I. Aaronson: *Surf. Sci.*, 1980, vol. 95, pp. 227-44.
23. Y.W. Lee and H.I. Aaronson: *Acta Metall.*, 1980, vol. 28, pp. 539-48.
24. W.L. Bragg and E.J. Williams: *Proc. R. Soc.*, 1934, vol. A145, pp. 699-730.
25. V. Kumar, D. Kumar, and S.K. Joshi: *Phys. Rev. B: Condens. Matter Mater. Phys.*, 1979, vol. B19, pp. 1954-62.
26. J.L. Moran-Lopez and L.M. Falicov: *Phys. Rev. B: Condens. Matter Mater. Phys.*, 1978, vol. B18, pp. 2542-48.
27. J.L. Moran-Lopez and L.M. Falicov: *Phys. Rev. B: Condens. Matter Mater. Phys.*, 1978, vol. B18, pp. 2549-54.
28. V. Kumar and K.H. Bennemann: *Phys. Rev. Lett.*, 1984, vol. 53, pp. 278-81.
29. J.M. Sanchez and J.L. Moran-Lopez: *Phys. Rev. B: Condens. Matter Mater. Phys.*, 1985, vol. B32, pp. 3534-40.
30. J.M. Sanchez and J.L. Moran-Lopez: *Surf. Sci.*, 1985, vol. 157, pp. L297-L302.
31. M. Polak and L. Rubinovich: *Surface Sci. Rep.*, 2000, vol. 38, pp. 127-94; *The Chemical Physics of Solid Surfaces*, D.P. Woodruff, ed., Elsevier Science, Amsterdam, 2002, vol. 10, pp. 86-117.
32. K. Lehovec: *J. Chem. Phys.*, 1953, vol. 21, pp. 1123-28.
33. K.L. Kliewer and J.S. Koehler: *Phys. Rev.*, 1965, vol. 140, pp. 1226-40.
34. P. Wynblatt and R.C. McCune: in *Surfaces and Interfaces in Ceramic and Metal-Ceramic Systems*, J.A. Pask and A.G. Evans, eds., Plenum, New York, NY, 1981, pp. 83-95.
35. P. Wynblatt and R.C. McCune: in *Surface and Near-Surface Chemistry of Oxide Materials*, J. Nowotny and L.-C. Dufour, eds., Elsevier Science Publishers, Amsterdam, 1988, pp. 247-79.
36. M. Guttmann: *Metall. Trans. A*, 1977, vol. 8A, pp. 1383-401.
37. M. Guttmann and D. McLean: in *Interfacial Segregation*, W.C. Johnson and J.M. Blakely, eds., ASM, Metals Park, OH, 1979, pp. 261-348.
38. M.A. Hoffmann and P. Wynblatt: *Metall. Trans. A*, 1989, vol. 20A, pp. 215-23.
39. P. Wynblatt and S.A. Dregia: *Coll. Phys. (suppl. J. Phys.)*, 1990, vol. 51-C1, pp. 757-66.
40. S.A. Dregia and P. Wynblatt: *Acta Metall. Mater.*, 1991, vol. 39, pp. 771-78.
41. G. Rao and P. Wynblatt: *Mater. Res. Soc. Symp. Proc.*, 1992, vol. 205, pp. 369-74.
42. D.A. Steigerwald, S.J. Miller, and P. Wynblatt: *Surf. Sci.*, 1985, vol. 155, pp. 79-100.
43. D. Wolf: *Acta Metall.*, 1989, vol. 37, pp. 1983-93.
44. D. Wolf: *Act Metall.*, 1989, vol. 37, pp. 2823-33.
45. D. Wolf: *Acta Metall. Mater.*, 1990, vol. 38, pp. 781-90.
46. P. Wynblatt, A. Saùl, and D. Chatain: *Acta Mater.*, 1998, vol. 46, pp. 2337-47.

47. D. Udler and D.N. Seidman: *Phys. Status Solidi*, 1992, vol. B172, pp. 267-85.
48. D. Udler and D.N. Seidman: *Acta Metall. Mater.*, 1994, vol. 42, pp. 1959-72.
49. S.M. Foiles, M.I. Baskes, and M.S. Daw: *Phys. Rev. B: Condens. Matter Mater. Phys.*, 1986, vol. B33, pp. 7983-91.
50. D. Chatain, N. Eustathopoulos, and P. Desré: *J. Coll. Interface Sci.*, 1981, vol. 83, pp. 384-92.
51. T.E. Faber: *Introduction to the Theory of Liquid Metals*, University Press, Cambridge, United Kingdom, 1972, pp. 128-29
52. A. Landa, P. Wynblatt, H. Hakkinen, R.N. Barnett, and U. Landman: *Phys. Rev. B: Condens. Matter Mater. Phys.*, 1995, vol. B51, pp. 10972-80.
53. F.L. Williams and D. Nason: *Surf. Sci.*, 1974, vol. 45, pp. 377-408.
54. C. Serre, P. Wynblatt, and D. Chatain: *Surf. Sci.*, 1998, vol. 415, pp. 336-45.
55. H. Shim, D. Chatain, and P. Wynblatt: *Surf. Sci.*, 1998, vol. 415, pp. 346-50.
56. P. Lejcek and S. Hofmann: *Crit. Rev. Solid State Mater. Sci.*, 1995, vol. 20, pp. 1-85.
57. S. Hofmann and P. Lejcek: *Interface Sci.*, 1996, vol. 3, pp. 241-67.
58. Y. Pang and P. Wynblatt: *J. Am. Ceram. Soc.*, 2005, vol. 88, pp. 2286-91.
59. P. Wynblatt and M. Takashima: *Proc. HTC-2000*, N. Eustathopoulos, K. Nogi, and N. Sobczak, eds., *Trans. JWRI*, 2001, vol. 30, pp. 11-20.
60. M. Ramamoorthy, D. Vanderbilt, and R.D. King-Smith: *Phys. Rev. B: Condens. Matter Mater. Phys.*, 1994, vol. B49, pp. 16721-27.
61. C.L. White and W.A. Coghlan: *Metall. Trans. A*, 1977, vol. 8A, pp. 1403-12.
62. P. Lejcek and S. Hofmann: *Interface Sci.*, 2002, vol. 9, pp. 221-30.
63. A.N. Aleshin, R.G. Faulkner, D.A. Molodov, and L.S. Shvindlerman: *Interface Sci.*, 2002, vol. 10, pp. 5-12.
64. M.P. Seah and C. Lea: *Philos. Mag.*, 1975, vol. 31, pp. 627-45.
65. H.J. Grabke: *Steel Res.*, 1986, vol. 57, pp. 178-85.
66. T. Muschik, S. Hofmann, W. Gust, and B. Predel: *Appl. Surf. Sci.*, 1989, vol. 37, pp. 439-55.
67. G.A. Lopez, W. Gust, and E.J. Mittemeijer: *Scripta Mater.*, 2003, vol. 49, pp. 747-53.
68. H. Mykura: *Acta Metall.*, 1961, vol. 9, pp. 570-76.
69. M. McLean and B. Gale: *Phil. Mag.*, 1969, vol. 20, pp. 1033-45.
70. G. Wulff: *Z. Krist. Mineral*, 1901, vol. 34, pp. 449-531.
71. C. Herring: in *Structure and Properties of Solid Surfaces*, R.G. Gomer and C.S. Smith, eds., University of Chicago Press, Chicago, IL, 1953, pp. 5-72.
72. J.C. Heyraud and J.J. Metois: *Surf. Sci.*, 1983, vol. 128, pp. 334-42.
73. J.C. Heyraud and J.J. Metois: *Acta Metall.*, 1980, vol. 28, pp. 1789-97.
74. J.C. Heyraud and J.J. Metois: *J. Cryst. Growth*, 1980, vol. 50, pp. 571-74.
75. Z. Wang and P. Wynblatt: *Surf. Sci.*, 1998, vol. 398, pp. 259-66.
76. D. Chatain, V. Ghetta, and P. Wynblatt: *Interface Sci.*, 2004, vol. 12, pp. 7-18.
77. E.D. Hondros and M. McLean: *Structures et Propriétés des Surfaces*, Editions du CNRS, Paris, 1970, pp. 219-29.
78. D. Chatain, P. Wynblatt, and G.S. Rohrer: *Acta Mater.*, 2005, vol. 53, pp. 4057-64.
79. W.-C. Cheng and P. Wynblatt: *J. Cryst. Growth*, 1997, vol. 173, pp. 513-27.
80. J.C. Heyraud and J.J. Metois: *J. Cryst. Growth*, 1987, vol. 82, pp. 269-73.
81. H.L. Meyerheim, H. Zajonz, W. Moritz, and I.K. Robinson: *Surf. Sci.*, 1997, vol. 381, pp. L551-57.
82. H.L. Meyerheim, M. DeSantis, W. Moritz, and I.K. Robinson: *Surf. Sci.*, 1998, vol. 418, pp. 295-302.
83. R. Roosen, R.P. McCormack, and W.C. Carter: *Comput. Mater. Sci.*, 1998, vol. 11, pp. 16-26.